The AP2 clathrin adaptor protein complex regulates the abundance of GLR-1 glutamate receptors in the ventral nerve cord of *Caenorhabditis elegans*

Steven D. Garafalo[a,b], Eric S. Luth[a], Benjamin J. Moss[a,c], Michael I. Monteiro[a,b], Emily Malkin[a], and Peter Juo[a]

[a]Department of Developmental, Molecular & Chemical Biology, [b]Graduate Program in Cellular and Molecular Physiology, and [c]Graduate Program in Neuroscience, Sackler School of Graduate Biomedical Sciences, Tufts University School of Medicine, Boston, MA 02111

ABSTRACT **Regulation of glutamate receptor (GluR) abundance at synapses by clathrin-mediated endocytosis can control synaptic strength and plasticity. We take advantage of viable, null mutations in subunits of the clathrin adaptor protein 2 (AP2) complex in *Caenorhabditis elegans* to characterize the in vivo role of AP2 in GluR trafficking. In contrast to our predictions for an endocytic adaptor, we found that levels of the GluR GLR-1 are decreased at synapses in the ventral nerve cord (VNC) of animals with mutations in the AP2 subunits APM-2/μ2, APA-2/α, or APS-2/σ2. Rescue experiments indicate that APM-2/μ2 functions in *glr-1*–expressing interneurons and the mature nervous system to promote GLR-1 levels in the VNC. Genetic analyses suggest that APM-2/μ2 acts upstream of GLR-1 endocytosis in the VNC. Consistent with this, GLR-1 accumulates in cell bodies of *apm-2* mutants. However, GLR-1 does not appear to accumulate at the plasma membrane of the cell body as expected, but instead accumulates in intracellular compartments including Syntaxin-13– and RAB-14–labeled endosomes. This study reveals a novel role for the AP2 clathrin adaptor in promoting the abundance of GluRs at synapses in vivo, and implicates AP2 in the regulation of GluR trafficking at an early step in the secretory pathway.**

Monitoring Editor
Anne Spang
University of Basel

Received: Jun 5, 2014
Revised: Mar 5, 2015
Accepted: Mar 6, 2015

INTRODUCTION

Alterations in glutamate receptor (GluR) levels at the synapse by activity-dependent exo- and endocytosis can alter synaptic strength and affect learning and memory (Shepherd and Huganir, 2007). The adaptor protein 2 (AP2) complex and clathrin function together at synapses to mediate activity-dependent endocytosis of mammalian AMPA-type GluRs (AMPARs) (Carroll *et al.*, 1999; Lüscher *et al.*, 1999; Lin *et al.*, 2000; Man *et al.*, 2000; Wang and Linden, 2000; Lee *et al.*, 2002). This AP2-dependent internalization of AMPARs is a critical mechanism underlying the induction of some forms of synaptic plasticity such as long-term depression (LTD) in hippocampal cultures (Man *et al.*, 2000; Lee *et al.*, 2002; Palmer *et al.*, 2005; Unoki *et al.*, 2012; Matsuda *et al.*, 2013) and in vivo (Griffiths *et al.*, 2008; Yoon *et al.*, 2009).

Membrane protein sorting and trafficking between various intracellular compartments and the plasma membrane is mediated by several distinct adaptor protein (AP) complexes (Owen *et al.*, 2004; Robinson, 2004). Five AP complexes, AP1–AP5, have been identified in mammals (Keen, 1987; Simpson *et al.*, 1997; Dell'Angelica *et al.*, 1999; Hirst *et al.*, 2011), whereas the *Caenorhabditis elegans* genome encodes two alternative AP1 complexes, one AP2 complex

This article was published online ahead of print in MBoC in Press (http://www.molbiolcell.org/cgi/doi/10.1091/mbc.E14-06-1048) on March 18, 2015.

Address correspondence to: Peter Juo (peter.juo@tufts.edu).

Abbreviations used: AMPARs, AMPA-type GluRs; AP2, adaptor protein 2; CME, clathrin-mediated endocytosis; dn, dominant-negative; FBS, fetal bovine serum; GFP, green fluorescent protein; GGA, Golgi-localized, gamma adaptin ear–containing, ARF-binding; GluR, glutamate receptor; HA, hemagglutinin; LTD, long-term depression; RFP, red fluorescent protein; ROI, region of interest; SV, synaptic vesicle; TGN, *trans*-Golgi network; VNC, ventral nerve cord.

and one AP3 complex (Lee *et al.*, 1994; Grant and Hirsh, 1999; Shim *et al.*, 2000; Shim and Lee, 2005). Each AP complex interacts with specific membrane phospholipids and protein cargoes via distinct sorting motifs to mediate vesicle formation at various intracellular membranes (Owen *et al.*, 2004). AP2 associates with the plasma membrane in part via its interaction with the plasma membrane–enriched phospholipid, phosphatidylinositol 4,5-bisphosphate (PtdIns(4,5)P_2) (Owen *et al.*, 2004) and regulates clathrin-mediated endocytosis (CME; McMahon and Boucrot, 2011). Similar to other AP complexes, AP2 is a heterotetramer consisting of two large subunits, α and β2; one medium subunit, μ2; and one small subunit, σ2. In rodent neurons, the μ2 subunit of AP2 binds to the cytosolic tail of GluR2 subunits and promotes the CME of AMPARs at synapses (Man *et al.*, 2000; Lee *et al.*, 2002; Kastning *et al.*, 2007). Acute treatment of neuronal cultures with peptides that interfere with AP2 binding to GluR2 can block AMPAR endocytosis and LTD (Lee *et al.*, 2002; Kastning *et al.*, 2007; Griffiths *et al.*, 2008; Yoon *et al.*, 2009). However, because knockout of AP2 subunits in mice and flies results in embryonic lethality (González-Gaitán and Jäckle, 1997; Mitsunari *et al.*, 2005), the in vivo role of AP2 in AMPAR trafficking has not been investigated. In this study, we take advantage of viable, null mutations and strong loss-of-function mutations in several AP2 subunits in *C. elegans* to investigate the role of AP2 in AMPAR trafficking in vivo.

The *C. elegans* AMPAR GLR-1 is expressed in interneurons, where it localizes to sensory-interneuron and interneuron-interneuron synapses (Hart *et al.*, 1995; Maricq *et al.*, 1995; Rongo *et al.*, 1998; Brockie *et al.*, 2001; Burbea *et al.*, 2002) and is required for several glutamate-dependent behaviors (Hart *et al.*, 1995; Maricq *et al.*, 1995; Zheng *et al.*, 1999; Mellem *et al.*, 2002; Chao *et al.*, 2004). In this study, we identify an unexpected role for the AP2 complex in GLR-1 trafficking. We find that in contrast to increased GLR-1 at synapses in the ventral nerve cord (VNC), as has been observed in other endocytic mutants such as *unc-11*/AP180 clathrin adaptin mutants (Burbea *et al.*, 2002), GLR-1 levels are reduced in the VNC of several AP2 subunit mutants. Although genetic analyses indicate that AP2 functions upstream of GLR-1 endocytosis in the VNC, the receptor does not accumulate at the plasma membrane of interneuron cell bodies as might be expected if CME were disrupted, but instead accumulates in intracellular compartments including Syntaxin-13– and RAB-14–labeled endosomes. This study characterizes, for the first time, the effect of AP2-null subunit mutations on GluR trafficking in vivo and reveals a novel role for AP2 in regulating GluR trafficking early in the secretory pathway.

RESULTS

AP2 functions in interneurons to promote GLR-1 abundance in the VNC

We use the genetic model organism *C. elegans* to identify genes and mechanisms that regulate AMPAR trafficking in vivo. We analyze the abundance of the AMPAR GLR-1 at synapses by measuring the distribution of a green fluorescent protein (GFP)-tagged version of GLR-1 (GLR-1::GFP). When expressed under the *glr-1* promoter, GLR-1::GFP localizes in a punctate pattern within VNC interneurons (Rongo *et al.*, 1998). More than 80% of these GLR-1::GFP puncta are closely apposed by presynaptic markers, suggesting that GLR-1::GFP is localized to postsynaptic sites (Rongo *et al.*, 1998; Burbea *et al.*, 2002). Additionally, expression of GLR-1::GFP under the *glr-1* promoter rescues the behavioral defects of *glr-1*–null mutants, indicating that GLR-1::GFP forms a functional receptor (Rongo *et al.*, 1998).

The abundance of mammalian AMPARs at the postsynaptic membrane is regulated by the clathrin adaptor AP2 and CME (Carroll *et al.*, 1999; Lüscher *et al.*, 1999; Lin *et al.*, 2000; Man *et al.*, 2000; Wang and Linden, 2000; Lee *et al.*, 2002; Kastning *et al.*, 2007). In *C. elegans*, disruption of the gene encoding the clathrin adaptin *unc-11/AP180* causes defects in CME (Zhang *et al.*, 1998; Nonet *et al.*, 1999) and, subsequently, increased levels of GLR-1::GFP in the VNC (Burbea *et al.*, 2002). We tested whether the clathrin adaptor AP2 was also involved in endocytosis of GLR-1 in the VNC by analyzing the abundance of GLR-1::GFP in animals with loss-of-function mutations in the μ2 subunit of AP2, *apm-2* (also known as *dpy-23*). Surprisingly, we found that GLR-1::GFP puncta fluorescence intensity decreases by 26% ($p < 0.001$) in *apm-2(gm17)*/μ2 loss-of-function mutants compared with wild-type controls (Figure 1, A, B, and H; see *Materials and Methods* for quantification). The *apm-2* mutation had a similar effect on GLR-1::GFP in a *glr-1(n2461)*–null mutant background (unpublished data). Histogram analysis shows that GLR-1::GFP puncta intensities decrease in *apm-2* mutants across the entire population of VNC puncta analyzed (Figure 1I). In addition, mutations in a second independent null allele of *apm-2*(*e840*)/μ2 exhibited a 30% decrease in GLR-1::GFP in the VNC ($p < 0.001$; Figure 1, A, D, and H). Expression of mCherry-tagged *apm-2* or untagged *apm-2* cDNA under control of the *glr-1* promoter corrects the GLR-1::GFP reduction observed in *apm-2*(*gm17*) or *apm-2(e840)* mutants, respectively (Figure 1, C, E, H, and I). These unexpected results led us to test whether the APM-2/μ2 subunit was functioning independently of the AP2 complex to regulate GLR-1 or whether other subunits of the AP2 complex contributed to this process. We found that loss-of-function mutants for the α subunit, *apa-2*(*ox422*), or the σ2 subunit, *aps-2*(*tm2912*), also had decreased GLR-1::GFP levels in the VNC ($p < 0.001$), and this effect was similar in magnitude (32–40%) to that observed in *apm-2* mutants (Figure 1). We did not analyze AP2 β subunit (*apb-1*) mutants, because this subunit is shared between the AP1 and AP2 complexes in *C. elegans* (Shim and Lee, 2000; Boehm and Bonifacino, 2001). We also found that loss-of-function mutations in other adaptor proteins that act early in the secretory pathway, including the Golgi-localized AP1 subunit *apm-1*/μ1 (Shafaq-Zadah *et al.*, 2012) or the sole *C. elegans* GGA (Golgi-localized, gamma adaptin ear–containing, ARF-binding) adaptor protein *apt-9*/GGA (Boehm and Bonifacino, 2001) had no effect ($p > 0.05$) on GLR-1::GFP puncta intensities in the VNC (Supplemental Figure S1). Taken together, these results indicate that AP2 functions in *glr-1*–expressing interneurons to promote GLR-1 abundance in the VNC.

We tested whether the effects of AP2 mutation on GLR-1 were specific or whether AP2 mutation also reduced the abundance of other neurotransmitter receptors at synapses, such as the AChR α7 subunit ACR-16 (Francis *et al.*, 2005) and the GABAR subunit UNC-49 (Bamber *et al.*, 1999) at the neuromuscular junction (Bamber *et al.*, 1999). We found that the fluorescence intensity of GFP-tagged ACR-16 and GFP-tagged UNC-49 increased at the neuromuscular junction of *apm-2* mutants (Supplemental Figure S2). These results are consistent with the predicted role of AP2 in endocytosis at the synaptic plasma membrane and suggest that the ability of AP2 to promote GLR-1 levels in the VNC may be relatively specific.

glr-1 transcript levels are not reduced in *apm-2* mutants

We tested whether the reduction in GLR-1::GFP observed in the VNC of AP2 subunit mutants was due to decreased transcription of *glr-1*. We measured the amount of *glr-1* mRNA relative to *act-1* (*actin*) mRNA by real-time PCR in wild type and *apm-2*(*gm17*) mutants. Instead of a decrease in *glr-1* transcript levels, we observed a 2.3-fold increase in *glr-1* mRNA in *apm-2*(*gm17*) mutants ($p < 0.01$)

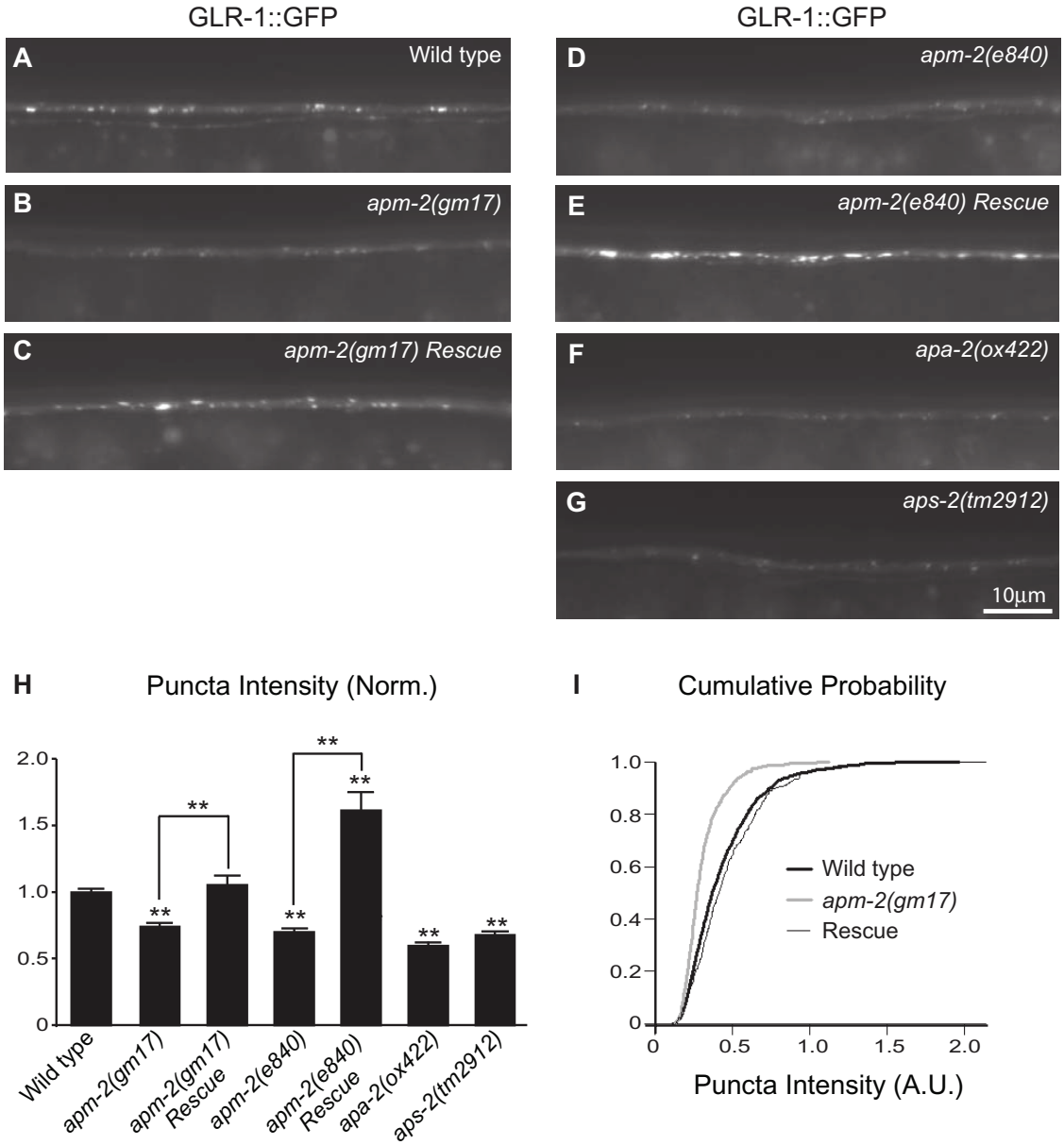

FIGURE 1: The clathrin adaptor AP2 promotes the abundance of GLR-1 in the VNC. (A–G) Representative images of GLR-1::GFP puncta in the anterior VNC of L4 wild-type (A), *apm-2*(*gm17*) (B), *Pglr-1::mCherry::apm-2* rescued *apm-2*(*gm17*) (C), *apm-2*(*e840*) (D), *Pglr-1::apm-2* rescued *apm-2*(*e840*) (E), *apa-2*(*ox422*) (F), and *aps-2*(*tm2912*) (G) animals expressing integrated GLR-1::GFP (*nuIs24*). All animals are oriented with anterior to the left and ventral to the top in these and all subsequent images (unless indicated otherwise). (H) Quantification of GLR-1::GFP puncta intensities (Norm., normalized) for the strains pictured in A–G. Shown are the means and SEMs for $n = 121$ wild-type, $n = 57$ *apm-2*(*gm17*), $n = 21$ *Pglr-1::mCherry::apm-2* rescued *apm-2*(*gm17*) animals, $n = 60$ *apm-2*(*e840*), $n = 27$ *Pglr-1::apm-2* rescued *apm-2*(*e840*), $n = 25$ *apa-2*(*ox422*), and $n = 31$ *aps-2*(*tm2912*). Values that differ significantly from wild type are indicated by asterisks above each bar, whereas other comparisons are marked by brackets (**, $p < 0.001$, Tukey-Kramer test). (I) Cumulative probability histogram of GLR-1::GFP puncta intensities (based on individual puncta intensities) for wild-type (thick black line), *apm-2(gm17)* (gray line), and *Pglr-1::mCherry::apm-2* rescued *apm-2*(*gm17*) (Rescue) (thin black line) animals ($p < 0.001$ for wild type vs. *apm-2(gm17)*; $p < 0.001$ for *apm-2(gm17)* vs. Rescue; $p > 0.05$ for wild type vs. Rescue, Kolmogorov-Smirnov test).

compared with wild-type controls (Figure 2). The increase in *glr-1* mRNA may suggest a potential feedback mechanism in which reductions in synaptic GLR-1 trigger increases in *glr-1* transcription. Nevertheless, this result indicates that the decrease in GLR-1::GFP in the VNC of *apm-2* mutants is not due to a reduction in *glr-1* transcript levels.

The decrease in GLR-1 in the VNC of *apm-2* mutants is not due to presynaptic changes in the number of synaptic vesicles

AP2 regulates synaptic vesicle (SV) endocytosis and recycling in neurons of *C. elegans*, *Drosophila*, and mammals (González-Gaitán and Jäckle, 1997; Gu *et al.*, 2008, 2013; Dittman and Ryan,

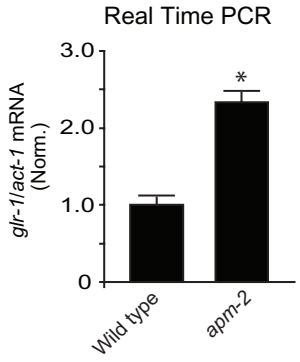

FIGURE 2: GLR-1 mRNA levels are not reduced in *apm-2* mutants. Real-time PCR analysis of mRNA levels in mixed-stage populations of wild-type and *apm-2*(*gm17*) animals expressing GLR-1::GFP (*nuIs24*). *glr-1* and *act-1* mRNA were detected by linear-range PCR amplification of total cDNA from each strain using gene-specific primers. Graph depicts the mean *glr-1* to *act-1* ratio ($n = 9$ replicates from three independent mRNA preps for each genotype) (Norm., normalized). Error bars show SEM. Values that differ significantly from wild type are indicated by an asterisk (*, $p < 0.01$, Student's *t* test).

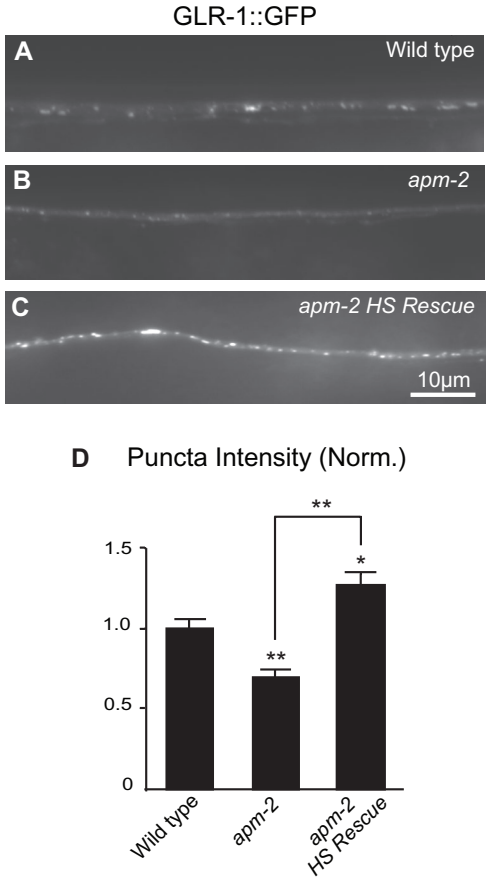

FIGURE 3: APM-2 can act in the mature nervous system to regulate the abundance of GLR-1 in the VNC. (A–C) Representative images of the anterior VNC of adult wild-type (A), *apm-2*(*gm17*) (B), and heat-shock rescued *apm-2*(*gm17*) (C) animals expressing GLR-1::GFP (*nuIs24*) after 2.5 h of heat shock and 17.5 h of recovery. Heat-shock rescued *apm-2* mutant animals express wild-type *apm-2* cDNA under control of a heat shock–inducible promoter (*pzEx259*). (D) Quantification of GLR-1::GFP puncta intensities (Norm., normalized) for the strains pictured in A–C. Graph depicts mean and SEMs for $n = 29$ wild-type, $n = 24$ *apm-2*(*gm17*), and $n = 27$ heat shock–rescued *apm-2*(*gm17*) animals. Values that differ significantly from wild type are indicated by asterisks above each bar, whereas other comparisons are marked by brackets (*, $p < 0.01$, **, $p < 0.001$, Tukey-Kramer test).

2009). In *C. elegans*, the number of SVs at presynaptic nerve terminals in motor neurons is greatly reduced in *apm-2* mutants (Gu *et al.*, 2008, 2013). Because alterations in presynaptic activity can lead to changes in postsynaptic GLR-1 levels (Grunwald *et al.*, 2004), we conducted two experiments to test whether the effects of *apm-2* on SV numbers could indirectly affect GLR-1 in the VNC. First, we measured the abundance of GLR-1::GFP in the VNC of animals containing mutations in the *C. elegans* Stonin orthologue *unc*-41 (Mullen *et al.*, 2012). Stonin family proteins interact with endocytic machinery and have been implicated in mediating SV endocytosis and recycling in *C. elegans*, *Drosophila*, and mammals (Fergestad *et al.*, 1999; Martina *et al.*, 2001; Walther *et al.*, 2004; Kelly and Phillips, 2005; Diril *et al.*, 2006). In *C. elegans*, *unc-41* mutants exhibit reductions in SV numbers at presynaptic sites that are almost identical to *apm-2* mutants (Gu *et al.*, 2008; Mullen *et al.*, 2012). Furthermore, *unc-41; apm-2* double mutants have reductions in SV numbers that are indistinguishable from *unc-41* single mutants (Mullen *et al.*, 2012), indicating that *unc-41* and *apm-2* function in the same genetic pathway to regulate SV numbers. If the decrease in GLR-1::GFP in the VNC of *apm-2* mutants was due to a postsynaptic response to reduced SVs, then we would expect *unc-41* mutants to have a decrease in GLR-1::GFP in the VNC similar to that of *apm-2* mutants. In contrast, we found that GLR-1::GFP puncta intensities were unaltered in the VNC of *unc-41* mutants ($p > 0.05$) compared with wild-type controls (Supplemental Figure S3, A–C). These data suggest that the effect of AP2 on SV recycling cannot explain the decrease in GLR-1::GFP abundance in the VNC of *apm-2* mutants. We also measured the distribution of GLR-1::GFP in the VNC of *unc-104*/KIF1A mutants. UNC-104 is required to transport SVs to presynaptic terminals in *C. elegans* neurons (Hall and Hedgecock, 1991), and the SV marker SNB-1::GFP is absent from synapses in the VNC of *unc-104* mutants (Rongo *et al.*, 1998). We found no difference in the fluorescence intensity of GLR-1::GFP in the VNC of wild type and *unc-104* mutants (Supplemental Figure S3, D–F), consistent with findings from a previous study (Rongo *et al.*, 1998). Together, these data suggest that the decrease in GLR-1 in the VNC of *apm-2* is unlikely a secondary consequence of the presynaptic effects of AP2 on SV numbers.

APM-2 is not required during early development to regulate GLR-1 in the VNC

We next tested whether the decrease in GLR-1 abundance in the VNC of AP2 mutants was due to defects in early development. To test this, we expressed *apm-2* cDNA under a heat shock– inducible promoter (*hsp16.2*) in *apm-2*(*gm17*) mutants expressing GLR-1::GFP. We raised animals at 20°C until the larval stage 4 (L4) of development and then heat shocked them at 30°C for 2.5 h to induce expression of *apm-2* cDNA. Animals were subsequently shifted to 20°C for 17.5 h to recover before imaging of GLR-1::GFP in the VNC of adult animals. Under this temperature-shift paradigm, we found that *apm-2*(*gm17*) mutants exhibited a 30% decrease ($p < 0.001$) in GLR-1::GFP puncta intensities in the VNC compared with wild-type controls (Figure 3, A, B, and D), which is similar to that observed in non heat-shocked *apm-2* mutants (Figure 1). In contrast, heat shock of *apm-2*(*gm17*) mutants expressing *apm-2* (under control of the heat shock–inducible promoter) exhibited increased GLR-1::GFP puncta intensities in the VNC ($p < 0.01$; Figure 3, A, C, and D). These

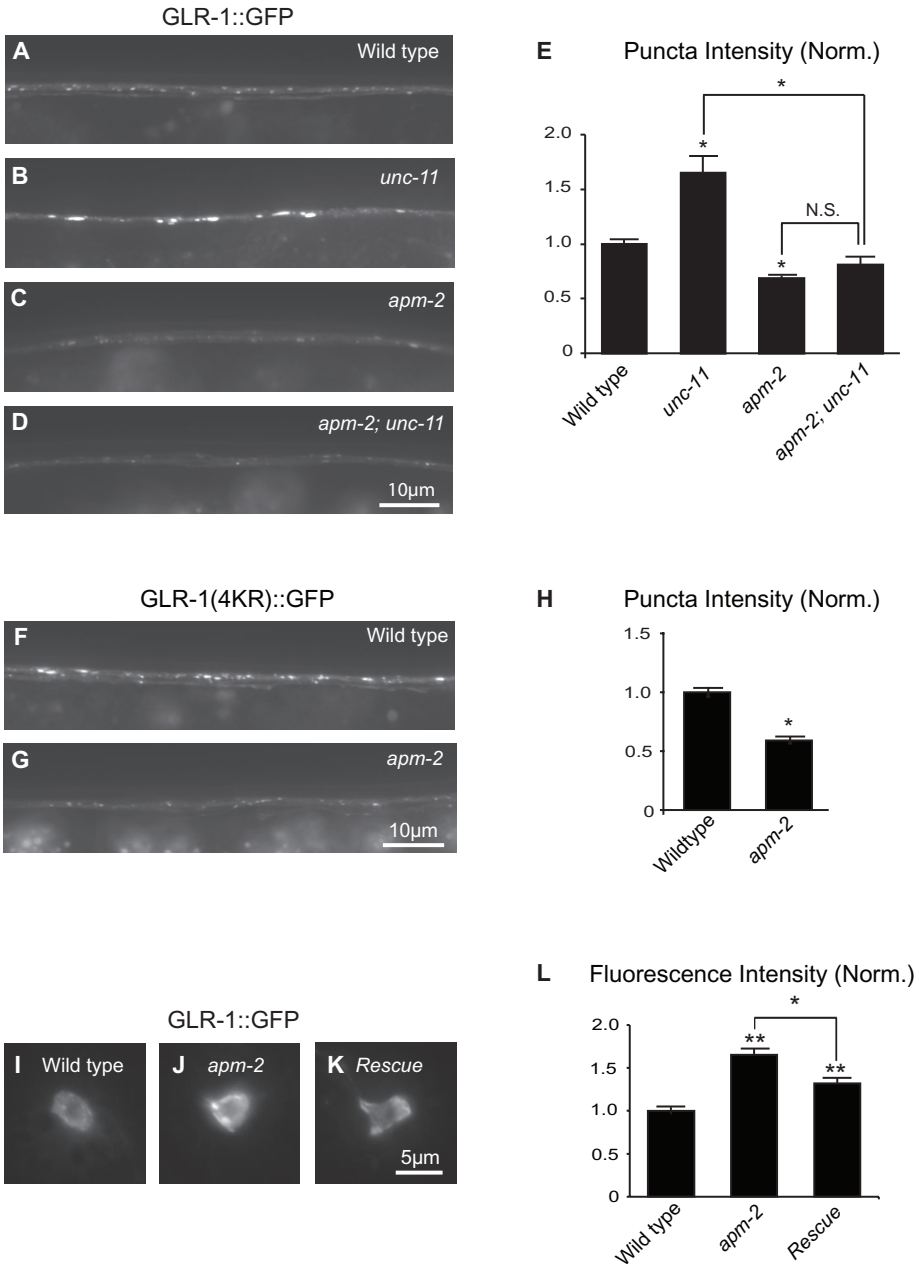

FIGURE 4: APM-2 functions upstream of GLR-1 endocytosis in the VNC. (A–D) Representative images of GLR-1::GFP puncta in the anterior VNC of L4 wild-type (A), *unc-11*(*e47*) (B), *apm-2*(*gm17*) (C), and *apm-2*(*gm17*); *unc-11*(*e47*) (D) animals expressing GLR-1::GFP (*nuIs24*). (E) Quantification of GLR-1::GFP puncta intensities (normalized) for the strains pictured in A–D. Shown are the means and SEMs for $n = 49$ wild-type, $n = 22$ *unc-11*(*e47*), $n = 57$ *apm-2*(*gm17*), and $n = 26$ *apm-2*(*gm17*); *unc-11*(*e47*) animals. Values that differ significantly from wild type are indicated by asterisks above each bar, whereas other comparisons are marked by brackets (*, $p < 0.01$, Tukey-Kramer test). N.S. denotes no significant difference ($p > 0.05$). (F and G) Representative images of the anterior VNC of L4 wild-type (F) and *apm-2*(*gm17*) (G) animals expressing integrated GLR-1(4KR)::GFP (*nuIs108*). (H) Quantification of GLR-1(4KR)::GFP puncta intensities (Norm., normalized) for the strains pictured in F and G. Shown are the means and SEMs for $n = 27$ wild-type and $n = 38$ *apm-2*(*gm17*) animals. (I–K) Representative images of PVC interneuron cell bodies of L4 wild-type (I), *apm-2*(*gm17*) (J), and *apm-2* rescued (K) animals expressing GLR-1::GFP (*nuIs24*). (L) Quantification of GLR-1::GFP mean fluorescence intensity (Norm., normalized) for the strains pictured in I–K. Shown are the means and SEM for $n = 27$ wild-type, $n = 24$ *apm-2*(*gm17*), and $n = 23$ *apm-2* rescued animals. Values that differ significantly from wild type are indicated by asterisks above each bar (*, $p < 0.01$, **, $p < 0.001$, Tukey-Kramer test).

results suggest that APM-2 is not required during early development to regulate GLR-1. These data also indicate that APM-2 can function in the adult nervous system to promote and maintain GLR-1 levels in the VNC.

APM-2 functions upstream of GLR-1 endocytosis in the VNC

GluRs are trafficked from the cell body to the VNC via vesicle-mediated transport and are subsequently delivered to the plasma membrane via exocytosis. At the synapse, GluRs are internalized via CME followed by either recycling back to the plasma membrane or degradation in the lysosome (Ehlers, 2000; Lin *et al.*, 2000; Shepherd and Huganir, 2007). The reduction in GLR-1 abundance in the VNC of AP2 mutants could arise from a decrease in anterograde trafficking of GLR-1 from the cell body to the VNC, a decrease in postendocytic receptor recycling, or an increase in postendocytic receptor degradation. We tested whether AP2 functions upstream of GLR-1 endocytosis in the VNC by measuring GLR-1::GFP distribution in the VNC of *apm-2; unc-11* double mutants. Mutations in the clathrin adaptin *unc-11/AP180* block CME (Zhang *et al.*, 1998; Nonet *et al.*, 1999) and result in increased GLR-1::GFP abundance in the VNC (Burbea *et al.*, 2002). If AP2 functions upstream of GLR-1 endocytosis in the VNC, then we would expect *apm-2; unc-11* double mutants to have a similar reduction in GLR-1::GFP puncta intensities in the VNC, as observed in *apm-2* single mutants. Conversely, if AP2 functions downstream of GLR-1 endocytosis in the VNC (i.e., to promote postendocytic recycling or inhibit degradation of GLR-1), then we would expect GLR-1::GFP to accumulate in the VNC of *apm-2; unc-11* double mutants to an extent similar to that found in *unc-11* single mutants. We found that *apm-2; unc-11* double mutants exhibit a decrease in GLR-1::GFP puncta intensities in the VNC similar to *apm-2* single mutants ($p = 0.6$; Figure 4, A–E). This result suggests that AP2 functions upstream of UNC-11/AP180–dependent endocytosis of GLR-1 in the VNC.

To further confirm that AP2 functions upstream of GLR-1 endocytosis and degradation in the VNC, we tested whether the levels of a nonubiquitinatable form of GFP-tagged GLR-1 (GLR-1(4KR)::GFP) are reduced in the VNC of *apm-2* mutants. Ubiquitination of GLR-1 promotes CME and degradation of the receptor (Burbea *et al.*, 2002). Mutation of all four lysines to arginines in the GLR-1 cytoplasmic tail prevents

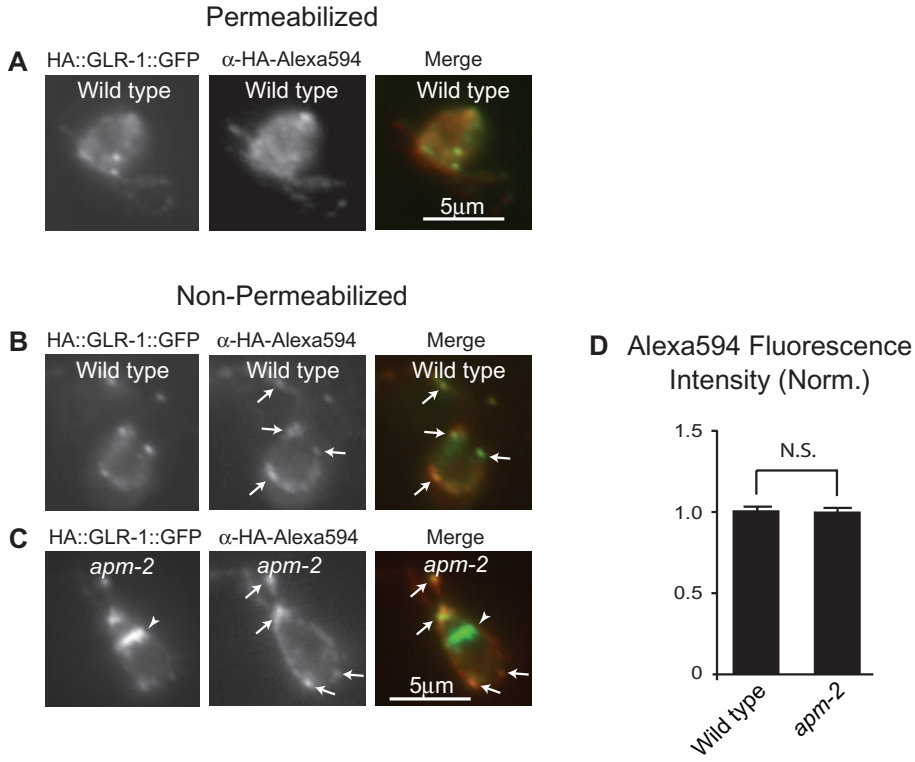

FIGURE 5: GLR-1 does not accumulate in the plasma membrane of the cell body of *apm-2* mutants. (A) Representative images of dissociated neurons under permeabilized conditions isolated from wild-type worms expressing an integrated extracellular HA-tagged GLR-1::GFP receptor (HA::GLR-1::GFP) (*pzIs12*). Shown are the GFP (left panel), Alexa Fluor 594 (middle panel), and merged (right panel) channels. (B and C) Representative images of dissociated neurons under nonpermeabilized conditions isolated from wild-type (B) and *apm-2*(*gm17*) (C) worms expressing HA::GLR-1::GFP (*pzIs12*). Shown are the GFP (left panel), Alexa Fluor 594 (middle panel), and merged (right panel) channels. (D) Quantification of Alexa Fluor 594 mean puncta fluorescence intensity (Norm., normalized) from the cell bodies of dissociated neurons for wild type and *apm-2*(*gm17*) mutants. Shown are the means and SEMs for $n = 30$ wild-type and $n = 30$ *apm-2*(*gm17*) animals. Arrows mark red, surface HA::GLR-1::GFP signal; the arrowhead marks green, internal HA::GLR-1::GFP. N.S. denotes no significant difference ($p > 0.05$, Student's *t* test).

ubiquitination and results in the accumulation of GLR-1(4KR)::GFP in the VNC (Burbea *et al.*, 2002). We found that GLR-1(4KR)::GFP fluorescence puncta intensities were decreased by 41% ($p < 0.001$) in the VNC of *apm-2* mutants compared with wild-type controls (Figure 4, F–H). This result is similar to the decrease of GLR-1::GFP observed in the VNC of *apm-2* mutants (Figure 1, A, B, D, and H). Taken together, these results suggest that AP2 functions upstream of GLR-1 endocytosis and postendocytic degradation in the VNC, consistent with a role for AP2 at an earlier trafficking step in the cell body.

GLR-1 accumulates in the neuronal cell bodies of APM-2 mutants

If AP2 regulates GLR-1 trafficking from the cell body to the synapse, then we would expect GLR-1 to accumulate in the interneuron cell bodies of AP2 subunit mutants. We tested this prediction by measuring the abundance of GLR-1::GFP in PVC interneuron cell bodies of *apa-2* and *apm-2* mutants. We found that GLR-1::GFP cell body fluorescence increased by 71% in *apa-2(ox422)* mutants (unpublished data) and by 65% in *apm-2* (*gm17*) mutants compared with wild-type controls ($p < 0.001$; Figure 4, I, J, and L). This accumulation was partially rescued by expression of wild-type *apm-2* cDNA (under control of the *glr-1* promoter) in *apm-2(gm17)* mutant neurons (Figure 4, I–L). These results indicate that GLR-1 abundance is increased in the cell body of AP2 subunit mutants, consistent with a role for AP2 in regulating an early step in GLR-1 trafficking from the cell body to the VNC.

GLR-1 does not accumulate at the plasma membrane of the cell body in *apm-2* mutants

Because GLR-1 decreases in the VNC and increases in the cell bodies of *apm-2* mutants, we tested whether AP2 mediates GLR-1 endocytosis at the plasma membrane of the cell body. In this model, GLR-1 would traffic from the Golgi to the plasma membrane of the cell body and be subsequently internalized via an AP2-dependent step before being trafficked to synapses in the VNC. In support of this idea, MHC class II receptors and lysosome-associated membrane proteins can be delivered to the plasma membrane before AP2-dependent endocytosis and subsequent trafficking to their target endosome and lysosome compartments, respectively (Dugast *et al.*, 2005; Janvier and Bonifacino, 2005; McCormick *et al.*, 2005). In addition, GLR-1 has been detected on the surface of interneuron cell bodies (Zheng *et al.*, 2004), but whether this plasma membrane pool of receptors are trafficked to the VNC in an AP2-dependent manner has not been tested.

To test whether APM-2 regulates GLR-1 levels at the surface of the cell body, we cultured neurons expressing GLR-1::GFP tagged with an extracellular hemagglutinin (HA) epitope (HA::GLR-1::GFP; Zheng *et al.*, 2004) isolated from wild-type and *apm-2(gm17)* mutant animals, as previously described (Christensen *et al.*, 2002; Zheng *et al.*, 2004; Strange *et al.*, 2007; see *Materials and Methods*). We measured surface HA::GLR-1::GFP levels with Alexa Fluor 594–conjugated anti-HA antibody under permeabilized and nonpermeabilized conditions. In control neurons, anti-HA–Alexa Fluor 594 antibody labeled only cell surface HA::GLR-1::GFP under nonpermeabilized conditions (Figure 5B), whereas the antibody labeled both surface and internal HA::GLR-1::GFP under permeabilized conditions (Figure 5A). Similar to the accumulation of GLR-1::GFP observed in *apm-2* mutant cell bodies in vivo (Figure 4, I–L), we found that HA::GLR-1::GFP abundance increased in the cell body of *apm-2*(*gm17*) mutant neurons in culture (Figure 5, B and C; Norm. wild type: 1.00 ± 0.08 SEM [$n = 30$], *apm-2*(*gm17*): 1.32 ± 0.11 SEM [$n = 30$], $p < 0.05$). We also found that surface HA::GLR-1::GFP levels at puncta in the neuronal processes of nonpermeablized neurons were reduced in *apm-2* mutants (average Alexa Fluor 594 puncta fluorescence intensity [Norm.]: wild type: 1.0 ± 0.09 [$n = 22$], *apm-2*: 0.72 ± 0.06 [$n = 20$], $p < 0.01$; unpublished data). These data suggest that *apm-2* mutant neurons in culture exhibit decreased surface GLR-1 along neuronal processes and increased accumulation of GLR-1 in cell bodies, recapitulating our in vivo data (Figures 1 and 4). Under nonpermeabilized conditions, we found that the average Alexa Fluor 594

fluorescence intensity was unaltered at the cell surface of *apm-2* mutants compared with wild-type controls ($p = 0.8$; Figure 5, B–D). Consistent with this result, we found that HA::GLR-1::GFP appears to accumulate in an internal compartment in *apm-2* mutant cell bodies (Figure 5C, arrowhead), resulting in a decreased surface to total HA::GLR-1::GFP ratio (average Alexa Fluor 594 fluorescence intensity/GFP intensity [Norm.]: wild type: 1.0 ± 0.06; *apm-2*: 0.69 ± 0.04, $p < 0.001$). These results indicate that GLR-1 levels at the plasma membrane of the cell body are unaltered in *apm-2* mutants, suggesting that AP2 does not function in GLR-1 endocytosis at the cell body surface.

GLR-1 partially accumulates in endosomes of *apm-2* mutants

Our data indicate that GLR-1::GFP accumulates in the cell bodies of *apm-2* mutants (Figures 4, I–L, and 5C), but not at the cell surface (Figure 5, B–D), suggesting that GLR-1 accumulates in an internal compartment of *apm-2* mutants. To identify this compartment, we analyzed the colocalization of GLR-1::GFP with a panel of red fluorescent protein (RFP)-tagged, compartment-specific markers using confocal microscopy (Chun *et al.*, 2008). These markers have previously been used to study GLR-1 trafficking through intracellular compartments (Chun *et al.*, 2008). We observed little colocalization between GLR-1::GFP and RFP-tagged compartment-specific SNARES, RFP::BET-1 (ERGIC), RFP::Syntaxin-5 (*cis*-Golgi), RFP::GOS-28 (Golgi), or RFP::Syntaxin-16 (*trans*-Golgi) in *apm-2* mutants (Figure 6, A–H). In contrast, we found strong colocalization between GLR-1::GFP and the early/recycling endosome markers RFP::Syntaxin-13 (Prekeris *et al.*, 1998; Figure 6, I and J) and mCherry::RAB-14 (Junutula *et al.*, 2004; Kelly *et al.*, 2010; Figure 6, K and L) in *apm-2* mutants. Although quantification revealed that there was no change in the percentage of GLR-1::GFP pixels colocalized with RFP::Syntaxin-13 or mCherry::RAB-14 in *apm-2* mutant cell bodies compared with wild-type controls (Figure 6, I–M; see *Materials and Methods*), we found that the mean intensity of GLR-1::GFP pixels colocalized with either RFP::Syntaxin-13– or mCherry::RAB-14–labeled endosomes increased by ~90% in *apm-2* mutants ($p < 0.001$) compared with wild-type controls (Figure 6N; see *Materials and Methods*). In contrast, we found no change in GLR-1::GFP pixel intensity in RFP::BET-1– or RFP::Syntaxin-16–labeled compartments in *apm-2* mutants (Figure 6N). Notably, we observed no change in the size of RFP::Syntaxin-13– (mean RFP::Syntaxin-13 pixel area [μm^2]: wild-type: 3.37 ± 0.23, *apm-2*: 4.21 ± 0.37, $p > 0.05$) or mCherry::RAB-14–labeled endosomes (mean mCherry::RAB-14 pixel area [μm^2]: wild type: 4.48 ± 0.56, *apm-2*: 3.83 ± 0.41, $p > 0.05$) in *apm-2* mutants compared with controls. The increase in GLR-1::GFP intensity in Syntaxin-13– and RAB-14–labeled compartments suggests that GLR-1 accumulates in endosomes in *apm-2* mutant cell bodies. In addition, we observed a decrease in the percentage of GLR-1::GFP pixels colocalized with the *trans*-Golgi network (TGN) marker RFP::Syntaxin-16 in *apm-2* mutants versus wild-type controls ($p < 0.01$; Figure 6, G, H, and M), whereas there was no change in the percentage of GLR-1::GFP colocalized with the ERGIC marker RFP::BET-1 ($p > 0.05$; Figure 6, A, B, and M). It should be noted that, in addition to the accumulation of GLR-1::GFP in Syntaxin-13– and RAB-14-labeled endosomes, we also observed an accumulation of GLR-1::GFP in another compartment that was not labeled by our panel of organelle markers and thus remains to be identified. Nevertheless, these results indicate that, in the absence of *apm-2*, GLR-1 accumulates in the cell body in internal compartments, including Syntaxin-13– and RAB-14–labeled endosomes.

Because the μ2 subunit of AP2 has been shown to interact with mammalian GluR2 receptors in vitro (Lee *et al.*, 2002; Kastning *et al.*, 2007), we tested whether APM-2::mCherry could colocalize with GLR-1::GFP in vivo. We found that APM-2::mCherry localized to puncta in interneuron cell bodies, and some of these puncta colocalized with GLR-1::GFP (Supplemental Figure S4). The accumulation of GLR-1 in intracellular compartments in *apm-2* mutants prompted us to test whether APM-2::GFP could localize to intracellular compartments labeled by our panel of RFP-tagged organelle markers described above. We found that APM-2::GFP partially colocalized with RFP::Syntaxin-13– (Figure 7A) and RFP::Syntaxin-16– (Figure 7B) labeled compartments, but not with RFP::Syntaxin-5– (Figure 7C) or RFP::GOS-28– (Figure 7D) labeled compartments. These data suggest that APM-2 can localize to intracellular compartments, where it may function to regulate GLR-1 trafficking.

The μ2 subunit of AP2 interacts in vitro with a stretch of basic amino acids in the cytoplasmic tail of rat GluR2, and this interaction is completely abolished by mutation of a single conserved basic residue, Lys-844 to alanine (Kastning *et al.*, 2007). Because this basic residue is conserved in the cytoplasmic tail of GLR-1 as Arg-887, we mutated this arginine to alanine (GLR-1(R887A)) to disrupt the predicted binding to μ2 and tested whether this point mutation would affect the trafficking of the receptor in wild-type animals. For this experiment, we generated transgenic lines expressing either GLR-1(WT)::GFP or GLR-1(R887A)::GFP at comparable levels as determined by Western blotting using anti-GFP antibodies on total worm lysates (Figure 8, A and B). To isolate the effects of the R887A mutation, we conducted our analysis in the background of a *glr-1; glr-2* double mutant, because endogenous GluR subunits have been shown to oligomerize with other mutant versions of GLR-1 and traffic them to the VNC (Chang and Rongo, 2005). We found that GLR-1(R887A)::GFP fluorescence decreased at puncta in the VNC (Figure 8, C and D; average puncta fluorescence [Norm.]: GLR-1(WT)::GFP: 1.0 ± 0.02 [$n = 30$], GLR-1(R887A)::GFP: 0.8 ± 0.04 [$n = 26$], $p \leq 0.01$), and increased in the cell body (Figure 8, E and F; average cell body fluorescence [Norm.]: GLR-1(WT)::GFP: 1.0 ± 0.04 [$n = 30$], GLR-1(R887A)::GFP: 1.3 ± 0.08 [$n = 26$], $p < 0.01$) of wild-type neurons relative to GLR-1(WT)::GFP. These effects were similar to those observed for wild-type GLR-1::GFP in the VNC and cell body of *apm-2* mutants (Figures 1 and 4). Furthermore, we compared the relative distributions of GLR-1(WT)::GFP and GLR-1(R887A)::GFP by calculating the ratio of GFP fluorescence in the VNC to the cell body to internally control for any potential differences in expression between the two transgenes. We found that the VNC to cell body ratio of GLR-1(R887A)::GFP fluorescence was reduced by 37% compared with the ratio of GLR-1(WT)::GFP (Figure 8G). These data are consistent with a model in which APM-2 functions at an internal compartment such as endosomes to promote GLR-1 trafficking from the cell body to the VNC.

DISCUSSION

Our data show that AP2 functions in interneurons to promote the abundance of GLR-1 at synapses in the VNC. We found that loss-of-function mutations in the AP2 subunits *apm-2*/μ2, *apa-2*/α, or *aps-2*/σ2 result in decreased levels of GLR-1::GFP in the VNC (Figure 1). The defect observed in *apm-2* mutants can be rescued by expression of wild-type *apm-2* cDNA in interneurons using the *glr-1* promoter (Figure 1). In addition, inducible expression of *apm-2* in the mature nervous system can rescue the reduction in GLR-1::GFP in the VNC (Figure 3), suggesting that APM-2 can function in adults to maintain GLR-1 levels. Genetic double-mutant analyses with the clathrin adaptin *unc-11*/AP180 suggest that AP2 acts upstream of GLR-1 endocytosis in the VNC. We found that mutations in *apm-2*/μ2 block the accumulation of GLR-1 observed in the VNC of

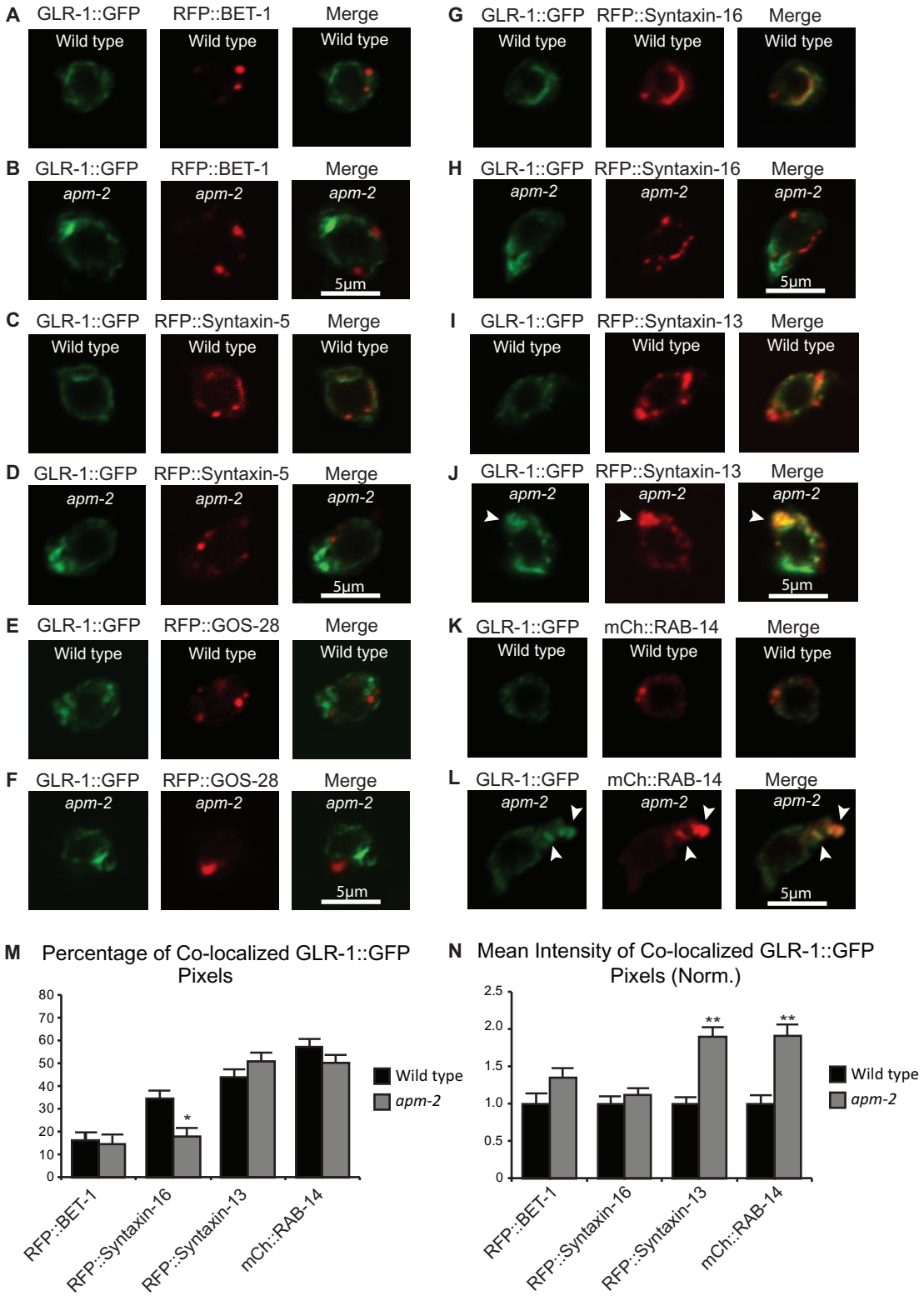

FIGURE 6: GLR-1 partially accumulates in Syntaxin-13– and RAB-14–positive compartments in the cell body of *apm-2* mutants. (A–L) Representative images of PVC interneuron cell bodies of L4 wild-type (A, C, E, G, I, and K) and *apm-2*(*gm17*) (B, D, F, H, J, and L) animals expressing GLR-1::GFP (*nuIs24*) and RFP-tagged markers for specific organelles including RFP::BET-1 (ERGIC) (A and B), RFP::Syntaxin-5 (*cis*-Golgi) (C and D), RFP::GOS-28 (Golgi) (E and F), RFP::Syntaxin-16 (*trans*-Golgi) (G and H), RFP::Syntaxin-13 (early/recycling endosomes) (I and J), and mCherry::RAB-14 (early/recycling endosomes) (K and L). (M) Quantification of the percentage of GLR-1::GFP pixels colocalized with RFP::BET-1, RFP::Syntaxin-16, RFP::Syntaxin-13 and mCherry::RAB-14 in wild-type and *apm-2*(*gm17*) animals. Graph depicts mean and SEM values for $n = 20$ wild type and $n = 24$ *apm-2* (*gm17*) for RFP::BET-1, $n = 23$ wild type and $n = 24$ *apm-2*(*gm17*) for RFP::Syntaxin-16, $n = 26$ wild type and $n = 33$ *apm-2* (*gm17*) for RFP::Syntaxin-13, and $n = 20$ wild type

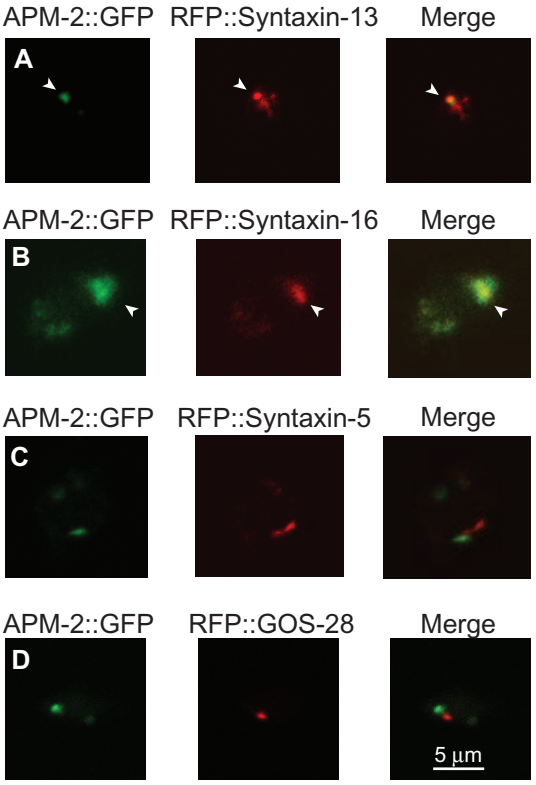

FIGURE 7: APM-2 localizes to intracellular compartments. (A–D) Representative confocal images of PVC interneuron cell bodies in L4 wild-type animals expressing APM-2::GFP and RFP-tagged markers for specific organelles including RFP::Syntaxin-13 (early and recycling endosomes) (A), RFP::Syntaxin-16 (*trans*-Golgi) (B), RFP::Syntaxin-5 (*cis*-Golgi) (C), and RFP::GOS-28 (Golgi) (D). Green channel (left panel), red channel (middle panel), and merged (right panel) images of cell bodies are shown for each pair of markers. Arrowheads indicate colocalization.

unc-11/AP180 endocytic mutants (Figure 4, A–E; Burbea *et al.*, 2002). Similarly, the VNC accumulation of a nonubiquitinatable version of GLR-1, GLR-1(4KR)::GFP (Burbea *et al.*, 2002), is reduced in *apm-2* mutants (Figure 4, F–H), suggesting that *apm-2* does not act at a postendocytic step to prevent GLR-1 degradation. These data suggest that AP2 acts upstream of GLR-1 endocytosis and postendocytic degradation in the VNC. Finally, GLR-1::GFP accumulates in cell bodies of *apm-2* mutants (Figure 4, I–L), consistent with the idea that AP2 regulates a trafficking step early in the secretory pathway to promote GLR-1 trafficking.

Our results were unexpected, because previous work using rodent neurons in culture demonstrated that AP2 functions at synapses to regulate CME of AMPARs (Lee *et al.*, 2002; Kastning *et al.*, 2007; Matsuda *et al.*, 2013). These studies utilized strategies that blocked but did not ablate AP2 function, including the use of inhibitory peptides to disrupt AP2 binding to AMPAR subunits (Lee *et al.*, 2002; Kastning *et al.*, 2007) or small interfering RNA to knock down specific AP2 subunits (Matsuda *et al.*, 2013). The effect of AP2 subunit mutants on GluR trafficking has not been studied in vivo, because null mutations in AP2 subunits in mice result in embryonic lethality (Mitsunari *et al.*, 2005). Thus, a role for AP2 in regulating GluR trafficking earlier in the secretory pathway in mammals may have been missed. In *C. elegans*, AP2 may also act at synapses to regulate GLR-1 endocytosis, but this role of AP2 may be masked in our subunit mutants, because AP2 is required at an earlier trafficking step in the cell body.

The µ2 subunit of AP2 can bind directly to an atypical motif in the cytoplasmic tail of mammalian GluR2 (Kastning *et al.*, 2007), and this motif is conserved in GLR-1 (Burbea *et al.*, 2002). Because AP2 is known to associate with the plasma membrane and regulate CME (Owen *et al.*, 2004; McMahon and Boucrot, 2011), and our data show that GLR-1 accumulates in the cell body of *apm-2* mutants (Figures 4–6), we tested whether GLR-1 accumulates at the plasma membrane in *apm-2* mutant cell bodies. In this model, GLR-1 would traffic from the Golgi to the surface of the cell body before being internalized by an AP2-dependent step and trafficked to the VNC. Indeed, several studies show that membrane proteins can traffic via the plasma membrane en route to their ultimate destination (Dugast *et al.*, 2005; Janvier and Bonifacino, 2005; McCormick *et al.*, 2005; Lasiecka and Winckler, 2011; Kaplan *et al.*, 2012). However, we did not observe an increase in HA-tagged GLR-1::GFP levels at the cell surface of *apm-2* mutant cell bodies (Figure 5). Instead, we found that GLR-1 accumulates in intracellular compartments in *apm-2* mutant cell bodies. Colocalization experiments with GLR-1::GFP and a panel of RFP-tagged organelle markers (Chun *et al.*, 2008) indicate that GLR-1 accumulates, in part, in Syntaxin-13– and RAB-14–labeled endosomes (Figure 6). These results illustrate that, in the absence of *apm-2*, GLR-1 is not efficiently trafficked to the VNC and accumulates in endosomes in the cell body.

Although AP2 does not appear to regulate surface levels of GLR-1 at the cell body, AP2 could still function in a canonical manner at the plasma membrane to indirectly regulate GLR-1 by controlling the internalization of another transmembrane protein required for forward GLR-1 trafficking. Indeed, AP2-dependent endocytosis of the Wnt secretion factor MIG-14/Wntless followed by retromer-dependent trafficking back to the Golgi is required for the forward trafficking of Wnt to the cell periphery in *C. elegans* (Bänziger *et al.*, 2006; Pan *et al.*, 2008), and retromer is required for GLR-1 trafficking (Zhang *et al.*, 2012). However, our data support a more direct role for AP2 in regulating GLR-1 trafficking. We found that APM-2 is localized to puncta that partially colocalize with GLR-1 (Supplemental Figure S4), the endosomal marker Syntaxin-13, and the TGN marker Syntaxin-16 (Figure 7). Furthermore, the distribution of GLR-1(R887A)::GFP, which contains a point mutation predicted to disrupt binding to µ2, phenocopies the distribution of wild-type GLR-1::GFP in *apm-2* mutants (i.e., decreases in the VNC and accumulates in the cell body of wild-type neurons; Figure 8). These data suggest that APM-2 can localize to intracellular compartments in the cell body, where it may function in a noncanonical manner to regulate some aspect of GLR-1 trafficking between the TGN and endosomal compartments.

and $n = 25$ *apm-2*(*gm17*) for mCherry::RAB-14. (N) Quantification of the mean intensity of GLR-1::GFP pixels colocalized with RFP::BET-1, RFP::Syntaxin-16, RFP::Syntaxin-13 and mCherry::RAB-14 (Norm., normalized) in wild-type and *apm-2*(*gm17*) animals. Graph depicts mean and SEM values for the *n* values indicated for M. Arrowheads indicate strong colocalization. Values that differ significantly from wild type are indicated by asterisks above each bar (*, $p < 0.01$, **, $p < 0.001$, Student's *t* test).

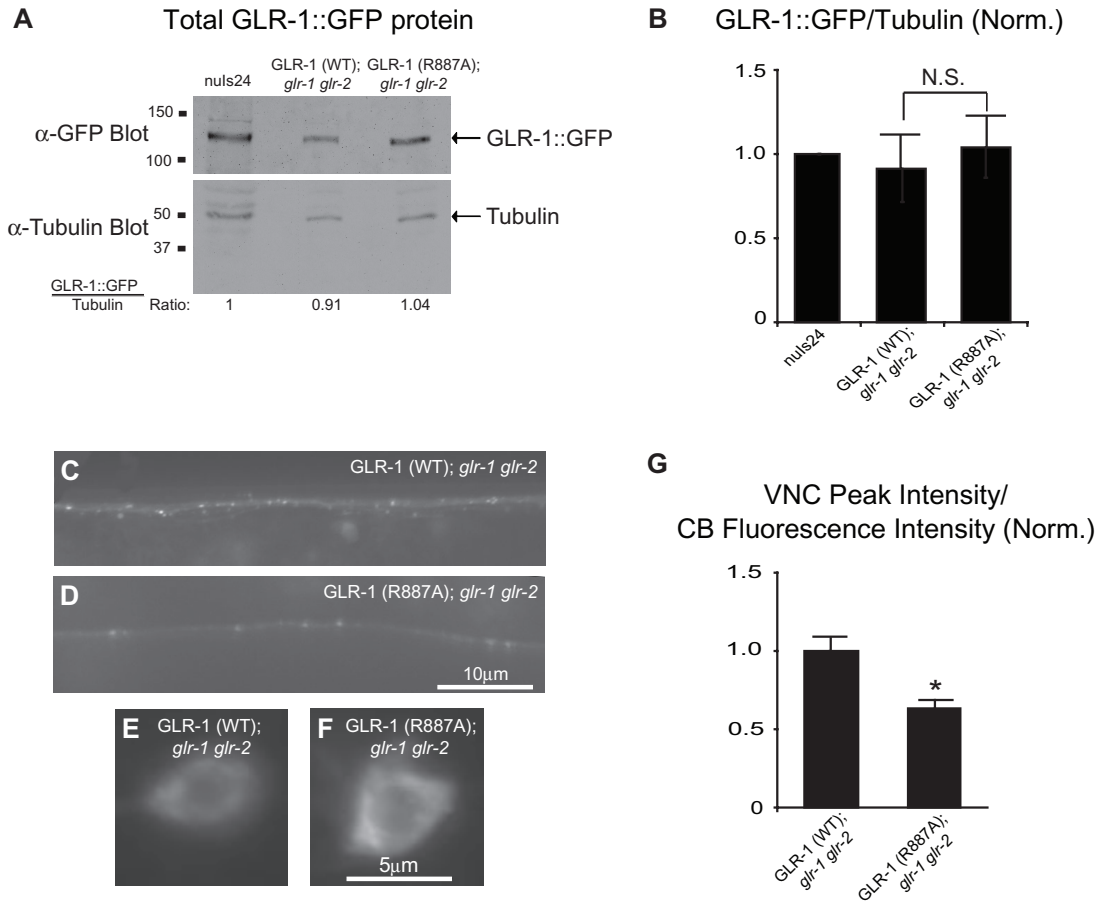

FIGURE 8: GLR-1(R887A)::GFP accumulates in the cell body and decreases in the VNC. (A) Western blot probed with anti-GFP antibodies (top gel) and antitubulin antibodies (bottom gel) of total worm lysates from the indicated strains showing comparable levels of transgene expression. The ratio of each GLR-1::GFP transgene to tubulin is indicated at the bottom of the gel and graphed in B from three independent lysates of each strain. The ratio for *nuIs24* was normalized (Norm.) to one. (C and D) Representative images of the anterior VNC of L4 *glr-1*(*ky176*) *glr-2*(*ak10*) animals expressing GLR-1(WT)::GFP (*pzEx223*) (C) or GLR-1(R887A)::GFP (*pzEx214*) (D). (E and F) Representative images of PVC interneuron cell bodies of L4 *glr-1*(*ky176*) *glr-2*(*ak10*) animals expressing GLR-1(WT)::GFP (*pzEx223*) (E) or GLR-1(R887A)::GFP (*pzEx214*) (F). (G) Quantification of the ratio of GLR-1::GFP mean fluorescence intensity in the VNC to the cell body for the strains pictured in C–F. Shown are the normalized (Norm.) ratios and SEM for $n = 30$ GLR-1(WT)::GFP and $n = 26$ GLR-1(R887A)::GFP–expressing animals. Values that differ significantly are indicated by an asterisk (*, $p < 0.01$).

We tested whether clathrin might function together with AP2 to regulate GLR-1 by expressing a dominant-negative (dn) version of clathrin heavy chain (clathrin hub mutant) that is known to disrupt clathrin function (Liu *et al.*, 1998). In contrast to AP2 subunit mutants, expression of dn-clathrin results in increased levels of GLR-1::GFP in the VNC (Supplemental Figure S5). These data could suggest that AP2 regulation of GLR-1 trafficking does not require clathrin, since AP2 subunit mutants and dn-clathrin expression result in distinct phenotypes. However, we favor an alternative interpretation, wherein clathrin functions together with UNC-101/μ1 (one of two alternative μ1 subunits of AP1) to regulate GLR-1 trafficking at a step before AP2 function. A previous study showed that GLR-1::GFP mislocalizes to presynaptic regions of the polarized neuron RIA in *unc-101*/μ1 mutants (Margeta *et al.*, 2009). We found that GLR-1::GFP increases in the VNC of *unc-101*/μ1 mutants similar to dn-clathrin–expressing animals (Supplemental Figure S5). Because the VNC interneurons are unipolar and have pre- and postsynaptic regions along the VNC, we speculate that GLR-1::GFP is mislocalized, perhaps to presynaptic regions in the VNC of *unc-101*/μ1 and dn-clathrin–expressing animals. Genetic double-mutant analysis revealed that expression of dn-clathrin or mutation of *unc-101*/μ1 completely block the reduction of GLR-1 observed in the VNC of *apm-2* single mutants (Supplemental Figure S5). These data suggest that *unc-101*/μ1 and clathrin function upstream of AP2 to regulate GLR-1 trafficking and are consistent with a model whereby disruption of clathrin or *unc-101*/μ1 results in mislocalization of GLR-1. This model is supported by several other studies demonstrating that, in the absence of AP1 function, target cargoes can become rerouted to alternate cellular destinations. For example, in *C. elegans*, mutations in *unc-101*/μ1 result in missorting of the ODR-10 odorant receptor and transient receptor potential channels from neuronal sensory cilia to axons of chemosensory neurons (Dwyer *et al.*, 2001; Bae *et al.*, 2006). Similarly, in mammalian hippocampal neurons, disruption of AP1 results in the mislocalization of *N*-methyl-D-aspartate receptor subunits to axons, and disruption of AP1 and clathrin result in the misincorporation of transferrin receptors into

axonal carriers and inappropriate trafficking to axons (Farias *et al.*, 2012). Clathrin may still function with AP2 at an intracellular compartment to regulate GLR-1 trafficking; however, the requirement for clathrin and AP1 at an earlier trafficking step precludes our ability to test this idea.

While localization of AP2 to the plasma membrane is largely dependent on its interaction with the phosphoinositide PtdIns(4,5)P_2, which is enriched in the plasma membrane (Di Paolo and De Camilli, 2006), several studies suggest that PtdIns(4,5)P_2 and AP2 may also function on intracellular compartments. For example, low levels of PtdIns(4,5)P_2 can be detected on several organelles, including the Golgi, endosomes, and lysosomes (Traub *et al.*, 1996; Arneson *et al.*, 1999; Watt *et al.*, 2002), and the kinases and phosphatases that regulate PtdIns(4,5)P_2 turnover have been found at the Golgi (Godi *et al.*, 1999; Jones *et al.*, 2000; De Matteis *et al.*, 2002; Choudhury *et al.*, 2005; Hyvola *et al.*, 2006). Interestingly, several noncanonical roles for AP2 have begun to emerge. A recent study in *C. elegans* showed that AP2 and clathrin function in a noncanonical manner to regulate both the phagocytosis of apoptotic cells and the maturation of phagosomes (Chen *et al.*, 2013). Another recent study showed that AP2 and AP4 can localize to autolysosomes during macroautophagy. Phosphatidylinositol 5-kinase generates microdomains of PtdIns(4,5)P_2 on autolysosomes to recruit AP2 and AP4 during lysosome re-formation after macroautophagy (Rong *et al.*, 2012). Although macroautophagy is often associated with cellular stress or starvation, increasing evidence suggests that macroautophagy also occurs under normal growth conditions (Ravikumar *et al.*, 2010; Maday *et al.*, 2012). Because the *C. elegans* genome does not encode an AP4 complex, and AMPARs mislocalize to axons and accumulate in intracellular compartments resembling autophagosomes in AP4-deficient hippocampal neurons (Matsuda *et al.*, 2008), further study will be needed to determine whether AP2 regulation of macroautophagy contributes to GLR-1 trafficking in vivo.

In summary, the analysis of viable null and loss-of-function mutants in AP2 subunits in this study revealed a novel function for AP2 in regulating GluR trafficking at an early step in the secretory pathway. It will be interesting in the future to test whether this AP2-dependent trafficking step is regulated by neuronal activity as a mechanism to control synaptic GluR levels.

MATERIALS AND METHODS

Strains

The following strains were used in this study: N2 (Bristol), *nuIs24 (Pglr-1::glr-1::gfp)*, *nuIs25 (Pglr-1::glr-1::gfp)*, *nuIs108 (Pglr-1::glr-1(4kr)::gfp)*, *pzIs12 (Pglr-1::ha::glr-1::gfp)*, *oxIs22 (Punc-49::unc-49::gfp)*, *ufIs8 (Pmyo-3::acr-16::gfp)* (kindly provided by M. Francis [University of Massachusetts Medical School, Worcester, MA]), *pzEx74 (Pglr-1::apm-2)*, *pzEx201 (Pglr-1::apm-2::mcherry)*, *pzEx214 (Pglr-1::glr-1(r887a)::gfp)*, *pzEx223 (Pglr-1::glr-1::gfp)*, *pzEx235 (Pglr-1::apm-2::mcherry)*, *pzEx259 (Phsp-16.2::apm-2)*, *pzEx278 (Pvha-6::apm-1::mcherry)*, *pzEx283 (Pglr-1::dn-clathrin)*, *pzEx347 (Pglr-1::mcherry::rab-14)*, *nuEx1330 (Pglr-1::rfp::bet-1)*, *nuEx1331 (Pglr-1::rfp::gos-28)*, *nuEx1332 (Pglr-1::rfp::syntaxin-16)*, *nuEx1337 (Pglr-1::rfp::syntaxin-13)*, *nuEx1340 (Pglr-1::rfp::syntaxin-5)*, *apa-2 (ox422)* (kindly provided by E. Jorgensen [University of Utah, Salt Lake City, UT]), *apm-1 (ok2578)*, *apm-2 (gm17)*, *apm-2 (e840)*, *aps-2 (tm2912)*, *apt-9 (tm3776)*, *glr-1(n2461)*, *glr-1 (ky176)* and *glr-2 (ak10)* (kindly provided by A. V. Maricq [University of Utah, Salt Lake City, UT]), *unc-11 (e47)*, *unc-41 (e268)*, *unc-101 (m1)*, and *unc-104 (e1265)*. All strains were maintained at 20°C as previously described (Brenner, 1974).

Constructs, transgenes, and germ-line transformation

Plasmids were generated using standard recombinant DNA techniques, and transgenic strains were created by plasmid microinjection. Details are available upon request. *nuIs24*, *nuIs25*, *nuIs108*, *nuEx1329*, *nuEx1330*, *nuEx1331*, *nuEx1332*, *nuEx1337*, and *nuEx1340* (kindly provided by Josh Kaplan [Massachusetts General Hospital, Boston, MA]; Rongo *et al.*, 1998; Burbea *et al.*, 2002; Chun *et al.*, 2008), *oxIs22* (Bamber *et al.*, 1999), and *pzIs12* (Kowalski *et al.*, 2011) have been previously described. *Pglr-1::apm-2* (FJ#122) was made by PCR amplifying the *apm-2* coding sequence from N2 cDNA, and inserting into the pV6 expression vector using *Nhe*I/*Kpn*I restriction sites to create plasmid FJ#122. *pzEx74* was generated by injecting *Pglr-1::apm-2* at 25 ng/µl along with the coinjection marker *Pmyo2::nls::mcherry* at 10 ng/µl. *Pglr-1::apm-2::mcherry* (FJ#123) was created by subcloning mCherry flanked by *Not*I restriction sites into a plasmid containing *Pglr-1::apm-2* with a *Not*I restriction site engineered immediately before the *apm-2* stop codon. *pzEx235* was generated by injecting *Pglr-1::apm-2::mcherry* (FJ#123) at 50 ng/µl alongside the coinjection marker *Pmyo2::nls::mcherry* at 10 ng/µl. *Phsp-16.2::apm-2* (FJ#124) was generated by subcloning the *apm-2* coding sequence from *Pglr-1::apm-2* into the *Nhe*I/*Kpn*I restriction sites of the pPD49.78 expression vector, which contains the *hsp-16.2* heat shock–inducible promoter (gift from Andrew Fire, Stanford University, Palo Alto, CA). *pzEx259* was generated by injecting *Phsp-16.2::apm-2* at 25 ng/µl alongside the coinjection marker *Pmyo2::nls::mcherry* at 10 ng/µl. *Pvha-6::apm-1::mcherry* (FJ#125) was generated by subcloning a 2.9-kb of sequence immediately upstream of the start codon of *vha-6* (*Pvha-6*) into the pPD49.26 expression vector using *Hin*dIII/*Xba*I restriction sites. *Apm-1* coding sequence was then PCR amplified from N2 cDNA and inserted into the pPD49.26 expression vector immediately after *Pvha-6* using the *Nhe*I/*Kpn*I restriction sites. mCherry flanked by *Not*I restriction sites was then subcloned into the pPD49.26 expression vector containing *Pvha-6* and *apm-1* coding sequence immediately before the *apm-1* stop codon. *pzEx278* was generated by injecting *Pvha-6::apm-1::mcherry* at 25 ng/µl alongside the coinjection marker *Pmyo2::nls::mcherry* at 10 ng/µl. *Pglr-1::glr-1(r887a)::gfp* (FJ#127) was made by PCR amplifying a plasmid containing *Pglr-1::glr-1::gfp* (FJ#126) with primers containing a "GCG" sequence at the site corresponding to *glr-1* R887 (AGG), using a QuikChange site-directed mutagenesis kit (Agilent Technologies, Santa Clara, CA). The resulting plasmid was then digested with *Nco*I, and the ~2.8-kb fragment containing sequence encoding R887A was then subcloned into the *Nco*I digested *Pglr-1::glr-1::gfp* plasmid and subsequently sequenced. *pzEx214* was made by injecting *Pglr-1::glr-1(r887a)::gfp* at 50 ng/µl. *pzEx223* was made by injecting *Pglr-1::glr-1::gfp* at 50 ng/µl. The *glr-1* promoter used in *pzEx214* and *pzEx223* consists of a ~2.3-kb fragment which starts immediately 5′ from the start codon and ends just before a *Hin*dIII site. *Pglr-1::dn-clathrin* (chc-hub) was made by PCR amplifying a region of the *chc-1* (clathrin heavy chain) coding region corresponding to residues 1075–1681 (which are homologous to those reported in Liu *et al.*, 1998) from N2 cDNA, and subcloning the fragment under the control of the *glr-1* promoter in pV6 using the *Nhe*I/*Kpn*I restriction sites. *pzEx283* was generated by injecting *Pglr-1::dn-clathrin* at 25 ng/µl alongside the coinjection marker *Pmyo2::nls::cherry* at 10 ng/µl. *pzEx347* was made by injecting *Pglr-1:: mcherry::rab-14* (KP#1541, gift from Josh Kaplan) at 25 ng/µl alongside the coinjection marker *ttx-3::dsred* at 75 ng/µl.

Fluorescence imaging

All VNC imaging experiments were performed with a Carl Zeiss AxioImager M1 microscope (Oberkochen, Germany) with a

100× Plan-Apochromat objective (1.4 numerical aperture) with GFP and RFP filter cubes. Images were acquired with an Orca-ER charge-coupled device camera (Hamamatsu, Hamamatsu, Japan), using MetaMorph, version 7.1 software (Molecular Devices, Sunnyvale, CA). All L4 animals were immobilized with 30 mg/ml 2,3-butanedione monoxamine (Sigma-Aldrich, St. Louis, MO) for 6–8 min before imaging. For heat-shock rescue experiments, L4 animals were shifted from 20°C to 30°C for 2.5 h. After heat shock, animals recovered at 20°C for 17.5 h before imaging. All images were acquired from the anterior portion of the VNC, posterior to RIG and AVG neuronal cell bodies. To quantitate fluorescent puncta in the VNC, we made maximum-intensity projections of z-series stacks (1-µm depth). Exposure settings and gain were optimized to fill the 12-bit dynamic range without saturation and were set identically for all images acquired within an experiment with a given fluorescent marker. Line scans of VNC puncta were made using MetaMorph, version 6.0 software. Line-scan data were analyzed with Igor Pro, versions 5 and 6 (Wavemetrics, Portland, OR), using custom-written software (gift from Jeremy Dittman, Weill Cornell Medical College, New York) as described previously (Burbea *et al.*, 2002). For normalization of arc lamp output, the fluorescence intensity of 0.5-µm FluoSphere beads (Invitrogen, Carlsbad, CA) was measured for each day of imaging. Puncta intensities were normalized to the average bead intensity for the corresponding day. Graphs of puncta intensities display intensity values normalized to wild-type controls. Puncta widths were calculated by measuring the width of each punctum at 50% of the maximal peak fluorescence intensity. Puncta densities were measured by calculating the average number of puncta per 10 µm along the VNC. All imaging quantification in the VNC is reported with average ± SEM values, and statistical significance was determined using Student's *t* test for experiments with two genotypes or the Tukey-Kramer test for experiments comparing more than two genotypes. For quantification of the amount of total GLR-1::GFP or surface HA::GLR-1::GFP in neuronal cell bodies, images were taken of PVC cell bodies with GFP or RFP filters, and maximum-intensity projections were made from z-series stacks (2-µm depth) as previously described (Juo *et al.*, 2007; Kowalski *et al.*, 2011; Monteiro *et al.*, 2012). The average pixel intensities of three distinct regions of each cell body were measured using MetaMorph, version 6.0 software. All imaging quantification in PVC cell bodies is reported with average ± SEM values, and statistical significance was determined using Student's *t* test. To quantify the amount of total or surface HA::GLR-1::GFP in neuronal processes in *C. elegans* neuronal cultures, we first identified neurons with distinct, well-formed processes. Line scans of puncta in these processes were then generated and analyzed as described above.

Fluorescence imaging of GLR-1::GFP and the various RFP-tagged compartment markers or APM-2::mCherry in PVC interneuron cell bodies was performed using a Zeiss LSM510 confocal microscope with a 63× objective (NA 1.4). L4 animals were immobilized with 30 mg/ml 2,3-butanedione monoxamine as described above. Fluorescent puncta were quantitated from a single representative plane containing both GFP and RFP signals using Zeiss LSM, version 4.2 software. Zeiss LSM software was used to quantitate the percent colocalized and the mean intensity of GLR-1::GFP. Background thresholds were first applied to each image using the threshold function to eliminate background fluorescence before analysis of an image region of interest (ROI) drawn around the perimeter of the cell body. The percentage and mean intensity of GLR-1::GFP pixels colocalized with specific organelle markers within the image ROI were calculated in LSM software for each image. Mean percentage and intensity of colocalized GLR-1::GFP pixels were then calculated for each strain by averaging the percentage and mean intensity values determined for $n \geq 20$ animals. All imaging quantification in PVC cell bodies is reported as average ± SEM values, and statistical significance was determined using Student's *t* test.

Real-time PCR

Total RNA was isolated from mixed-stage wild-type (*nuIs24*) and *apm-2* mutant (*nuIs24*; *apm-2* (*gm17*)) strains using the RNeasy Fibrous Tissue Mini kit (Qiagen, Valencia, CA) as previously described (Kowalski *et al.*, 2011; Monteiro *et al.*, 2012). Three independent RNA preparations were isolated for each genotype. cDNA from these RNA preps was synthesized using Superscript III Reverse Transcriptase (Invitrogen). Real-time PCR was performed on the MX3000P real-time PCR machine (Tufts Center for Neuroscience Research, Boston, MA) using the Brilliant SYBR Green QPCR Master Mix and SureStart Taq (Stratagene, Santa Clara, CA). The relative amount of *glr-1* mRNA compared with *act-1* mRNA was determined as previously described (Pfaffl, 2001), after generating standard curves to calculate the efficiency of *glr-1* and *act-1* primers. The ratio of *glr-1* mRNA to *act-1* mRNA in *apm-2 (gm17)* mutants was normalized to that of wild-type animals with average ± SEM values reported. Statistical significance was determined using the Student's *t* test ($n = 3$ replicates of three independent cDNA preps for each genotype).

Primary culture of *C. elegans* neurons

Neurons were isolated from wild type and *apm-2* mutants expressing *Pglr-1::ha::glr-1::gfp* (*pzIs12*) and cultured as previously described (Christensen *et al.*, 2002; Strange *et al.*, 2007). Briefly, egg-bearing adult worms were collected from age-synchronized plates and washed with M9 buffer to remove bacteria. Worms were lysed in egg isolation solution (2N NaOH, 20% bleach) for 5 min and washed several times with egg buffer (118 mM NaCl, 48 mM KCl, 2 mM $CaCl_2$, 2 mM $MgCl_2$, 25 mM HEPES, pH 7.3). Eggs were harvested by sucrose float and digested under sterile conditions using chitinase (Sigma-Aldrich). Digested eggs were then resuspended in sterile L-15 medium (Invitrogen) containing 10% (vol/vol) heat-inactivated fetal bovine serum (FBS; Invitrogen), 50 U/ml penicillin (Invitrogen), and 50 µg/ml streptomycin (Invitrogen). Cells were then gently dissociated from the digested eggs by pipetting the cell suspension against the inside wall of a sterile microcentrifuge tube and were then filtered using a 5-µm Durapore syringe filter (Millipore, Bedford, MA). Cells were seeded onto 18-mm glass coverslips (Thermo Fisher Scientific, Waltham, MA) coated with peanut-lectin (Sigma-Aldrich) and grown in L-15 media with FBS, penicillin, and streptomycin. Cell cultures were maintained in humidified boxes at 20°C, and immunolabeling experiments were conducted 3–4 d postplating.

Immunolabeling

Primary cultured neurons were fixed and stained as previously described (Zheng *et al.*, 2004). Briefly, neurons were fixed in 3% paraformaldehyde at room temperature for 30 min. For labeling of surface HA::GLR-1::GFP receptors, cells were blocked in 0.2% bovine serum albumin for 20 min and then incubated with 0.5 µg/ml anti-HA–Alexa Fluor 594 antibodies (16B12; Invitrogen) for 45 min. For labeling of all HA::GLR-1::GFP receptors, neurons were permeabilized in 0.2% Triton X-100 for 2 min before blocking. Cells were then washed in phosphate-buffered saline and mounted onto glass slides for imaging.

ACKNOWLEDGMENTS

We thank Erik Jorgensen, Villu Maricq, Mike Francis, Jason McEwen, and Josh Kaplan for strains and plasmids and Steven Del Signore

and Victor Hatini for assistance and use of the Zeiss LSM510 confocal microscope. Some strains were provided by the Caenorhabditis Genetics Center, which is funded by the National Institutes of Health (NIH) Office of Research Infrastructure Programs (P40 OD010440), and the Mitani lab, which is funded by the National Bio-Resource Project. S.D.G. was supported in part by the Synapse Neurobiology Training Program (NIH grant T32 NS061764) and by a Pathobiology of Digestive Diseases grant (NIH grant T32 DK007542). E.S.L. was supported in part by the Training in Education and Critical Research Skills Postdoctoral Fellowship Program (NIH grant 5K12GM074869). M.I.M. was supported in part by a Genetics and Development Training grant (NIH grant 5K12GM074869). We thank the Juo lab for helpful discussions and critical reading of the manuscript. This research was supported by NIH grant NS059953 (P.J.), a National Science Foundation grant (IOS1353862), and the Tufts Center for Neuroscience Research (NIH grant P30 NS047243).

REFERENCES

Arneson LS, Kunz J, Anderson RA, Traub LM (1999). Coupled inositide phosphorylation and phospholipase D activation initiates clathrin-coat assembly on lysosomes. J Biol Chem 274, 17794–17805.

Bae Y-K, Qin H, Knobel KM, Hu J, Rosenbaum JL, Barr MM (2006). General and cell-type specific mechanisms target TRPP2/PKD-2 to cilia. Development 133, 3859–3870.

Bamber BA, Beg AA, Twyman RE, Jorgensen EM (1999). The *Caenorhabditis elegans* unc-49 locus encodes multiple subunits of a heteromultimeric GABA receptor. J Neurosci 19, 5348–5359.

Bänziger C, Soldini D, Schütt C, Zipperlen P, Hausmann G, Basler K (2006). Wntless, a conserved membrane protein dedicated to the secretion of Wnt proteins from signaling cells. Cell 125, 509–522.

Boehm M, Bonifacino JS (2001). Adaptins: the final recount. Mol Biol Cell 12, 2907–2920.

Brenner S (1974). The genetics of *Caenorhabditis elegans*. Genetics 77, 71–94.

Brockie PJ, Madsen DM, Zheng Y, Mellem J, Maricq AV (2001). Differential expression of glutamate receptor subunits in the nervous system of *Caenorhabditis elegans* and their regulation by the homeodomain protein UNC-42. J Neurosci 21, 1510–1522.

Burbea M, Dreier L, Dittman JS, Grunwald ME, Kaplan JM (2002). Ubiquitin and AP180 regulate the abundance of GLR-1 glutamate receptors at postsynaptic elements in *C. elegans*. Neuron 35, 107–120.

Carroll RC, Beattie EC, Xia H, Lüscher C, Altschuler Y, Nicoll RA, Malenka RC, von Zastrow M (1999). Dynamin-dependent endocytosis of ionotropic glutamate receptors. Proc Natl Acad Sci USA 96, 14112–14117.

Chang HC, Rongo C (2005). Cytosolic tail sequences and subunit interactions are critical for synaptic localization of glutamate receptors. J Cell Sci 118, 1945–1956.

Chao MY, Komatsu H, Fukuto HS, Dionne HM, Hart AC (2004). Feeding status and serotonin rapidly and reversibly modulate a *Caenorhabditis elegans* chemosensory circuit. Proc Natl Acad Sci USA 101, 15512–15517.

Chen D, Jian Y, Liu X, Zhang Y, Liang J, Qi X, Du H, Zou W, Chen L, Chai Y, *et al*. (2013). Clathrin and AP2 are required for phagocytic receptor-mediated apoptotic cell clearance in *Caenorhabditis elegans*. PLoS Genet 9, e1003517.

Choudhury RR, Hyvola N, Lowe M (2005). Phosphoinositides and membrane traffic at the *trans*-Golgi network. Biochem Soc Symp 31–38.

Christensen M, Estevez A, Yin X, Fox R, Morrison R, McDonnell M, Gleason C, Miller DM III, Strange K (2002). A primary culture system for functional analysis of *C. elegans* neurons and muscle cells. Neuron 33, 503–514.

Chun DK, McEwen JM, Burbea M, Kaplan JM (2008). UNC-108/Rab2 regulates postendocytic trafficking in *Caenorhabditis elegans*. Mol Biol Cell 19, 2682–2695.

Dell'Angelica EC, Mullins C, Bonifacino JS (1999). AP-4, a novel protein complex related to clathrin adaptors. J Biol Chem 274, 7278–7285.

De Matteis M, Godi A, Corda D (2002). Phosphoinositides and the Golgi complex. Curr Opin Cell Biol 14, 434–447.

Di Paolo G, De Camilli P (2006). Phosphoinositides in cell regulation and membrane dynamics. Nature 443, 651–657.

Diril MK, Wienisch M, Jung N, Klingauf J, Haucke V (2006). Stonin 2 is an AP-2-dependent endocytic sorting adaptor for synaptotagmin internalization and recycling. Dev Cell 10, 233–244.

Dittman J, Ryan TA (2009). Molecular circuitry of endocytosis at nerve terminals. Annu Rev Cell Dev Biol 25, 133–160.

Dugast M, Toussaint H, Dousset C, Benaroch P (2005). AP2 clathrin adaptor complex, but not AP1, controls the access of the major histocompatibility complex (MHC) class II to endosomes. J Biol Chem 280, 19656–19664.

Dwyer ND, Adler CE, Crump JG, L'Etoile ND, Bargmann CI (2001). Polarized dendritic transport and the AP-1 μ1 clathrin adaptor UNC-101 localize odorant receptors to olfactory cilia. Neuron 31, 277–287.

Ehlers MD (2000). Reinsertion or degradation of AMPA receptors determined by activity-dependent endocytic sorting. Neuron 28, 511–525.

Farías GG, Cuitino L, Guo X, Ren X, Jarnik M, Mattera R, Bonifacino JS (2012). Signal-mediated, AP-1/clathrin-dependent sorting of transmembrane receptors to the somatodendritic domain of hippocampal neurons. Neuron 75, 810–823.

Fergestad T, Davis WS, Broadie K (1999). The stoned proteins regulate synaptic vesicle recycling in the presynaptic terminal. J Neurosci 19, 5847–5860.

Francis MM, Evans SP, Jensen M, Madsen DM, Mancuso J, Norman KR, Maricq AV (2005). The Ror receptor tyrosine kinase CAM-1 is required for ACR-16-mediated synaptic transmission at the *C. elegans* neuromuscular junction. Neuron 46, 581–594.

Godi A, Pertile P, Meyers R, Marra P, Di Tullio G, Iurisci C, Luini A, Corda D, De Matteis MA (1999). ARF mediates recruitment of PtdIns-4-OH kinase-beta and stimulates synthesis of PtdIns(4,5)P2 on the Golgi complex. Nat Cell Biol 1, 280–287.

González-Gaitán M, Jäckle H (1997). Role of *Drosophila* alpha-adaptin in presynaptic vesicle recycling. Cell 88, 767–776.

Grant B, Hirsh D (1999). Receptor-mediated endocytosis in the *Caenorhabditis elegans* oocyte. Mol Biol Cell 10, 4311–4326.

Griffiths S, Scott H, Glover C, Bienemann A, Ghorbel MT, Uney J, Brown MW, Warburton EC, Bashir ZI (2008). Expression of long-term depression underlies visual recognition memory. Neuron 58, 186–194.

Grunwald ME, Mellem JE, Strutz N, Maricq AV, Kaplan JM (2004). Clathrin-mediated endocytosis is required for compensatory regulation of GLR-1 glutamate receptors after activity blockade. Proc Natl Acad Sci USA 101, 3190–3195.

Gu M, Liu Q, Watanabe S, Sun L, Hollopeter G, Grant BD, Jorgensen EM (2013). AP2 hemicomplexes contribute independently to synaptic vesicle endocytosis. eLife 2, e00190.

Gu M, Schuske K, Watanabe S, Liu Q, Baum P, Garriga G, Jorgensen EM (2008). μ2 adaptin facilitates but is not essential for synaptic vesicle recycling in *Caenorhabditis elegans*. J Cell Biol 183, 881–892.

Hall DH, Hedgecock EM (1991). Kinesin-related gene *unc-104* is required for axonal transport of synaptic vesicles in *C. elegans*. Cell 65, 837–847.

Hart AC, Sims S, Kaplan JM (1995). Synaptic code for sensory modalities revealed by *C. elegans* GLR-1 glutamate receptor. Nature 378, 82–85.

Hirst J, Barlow LD, Francisco GC, Sahlender DA, Seaman MNJ, Dacks JB, Robinson MS (2011). The fifth adaptor protein complex. PLoS Biol 9, e1001170.

Hyvola N, Diao A, McKenzie E, Skippen A, Cockcroft S, Lowe M (2006). Membrane targeting and activation of the Lowe syndrome protein OCRL1 by rab GTPases. EMBO J 25, 3750–3761.

Janvier K, Bonifacino JS (2005). Role of the endocytic machinery in the sorting of lysosome-associated membrane proteins. Mol Biol Cell 16, 4231–4242.

Jones DH, Morris JB, Morgan CP, Kondo H, Irvine RF, Cockcroft S (2000). Type I phosphatidylinositol 4-phosphate 5-kinase directly interacts with ADP-ribosylation factor 1 and is responsible for phosphatidylinositol 4,5-bisphosphate synthesis in the Golgi compartment. J Biol Chem 275, 13962–13966.

Junutula JR, De Maziere AM, Peden AA, Ervin KE, Advani RJ, van Dijk SM, Klumperman J, Scheller RH (2004). Rab14 is involved in membrane trafficking between the Golgi complex and endosomes. Mol Biol Cell 15, 2218–2229.

Juo P, Harbaugh T, Garriga G, Kaplan JM (2007). CDK-5 regulates the abundance of GLR-1 glutamate receptors in the ventral cord of *Caenorhabditis elegans*. Mol Biol Cell 18, 3883–3893.

Kaplan OI, Doroquez DB, Cevik S, Bowie RV, Clarke L, Sanders AAWM, Kida K, Rappoport JZ, Sengupta P, Blacque OE (2012). Endocytosis genes facilitate protein and membrane transport in *C. elegans* sensory cilia. Curr Biol 22, 451–460.

Kastning K, Kukhtina V, Kittler JT, Chen G, Pechstein A, Enders S, Lee SH, Sheng M, Yan Z, Haucke V (2007). Molecular determinants for the interaction between AMPA receptors and the clathrin adaptor complex AP-2. Proc Natl Acad Sci USA 104, 2991–2996.

Keen JH (1987). Clathrin assembly proteins: affinity purification and a model for coat assembly. J Cell Biol 105, 1989–1998.

Kelly EE, Horgan CP, Adams C, Patzer TM, Ni Shuilleabhain DM, Norman JC, McCaffrey MW (2010). Class I Rab11-family interacting proteins are binding targets for the Rab14 GTPase. Biol Cell 102, 51–62.
Kelly LE, Phillips AM (2005). Molecular and genetic characterization of the interactions between the *Drosophila* stoned-B protein and DAP-160 (intersectin). Biochem J 388, 195–204.
Kowalski JR, Dahlberg CL, Juo P (2011). The deubiquitinating enzyme USP-46 negatively regulates the degradation of glutamate receptors to control their abundance in the ventral nerve cord of *Caenorhabditis elegans*. J Neurosci 31, 1341–1354.
Lasiecka ZM, Winckler B (2011). Mechanisms of polarized membrane trafficking in neurons–focusing in on endosomes. Mol Cell Neurosci 48, 278–287.
Lee J, Jongeward GD, Sternberg PW (1994). *unc-101*, a gene required for many aspects of *Caenorhabditis elegans* development and behavior, encodes a clathrin-associated protein. Genes Dev 8, 60–73.
Lee SH, Liu L, Wang YT, Sheng M (2002). Clathrin adaptor AP2 and NSF interact with overlapping sites of GluR2 and play distinct roles in AMPA receptor trafficking and hippocampal LTD. Neuron 36, 661–674.
Lin JW, Ju W, Foster K, Lee SH, Ahmadian G, Wyszynski M, Wang YT, Sheng M (2000). Distinct molecular mechanisms and divergent endocytotic pathways of AMPA receptor internalization. Nat Neurosci 3, 1282–1290.
Liu SH, Marks MS, Brodsky FM (1998). A dominant-negative clathrin mutant differentially affects trafficking of molecules with distinct sorting motifs in the class II major histocompatibility complex (MHC) pathway. J Cell Biol 140, 1023–1037.
Lüscher C, Xia H, Beattie EC, Carroll RC, von Zastrow M, Malenka RC, Nicoll RA (1999). Role of AMPA receptor cycling in synaptic transmission and plasticity. Neuron 24, 649–658.
Maday S, Wallace KE, Holzbaur ELF (2012). Autophagosomes initiate distally and mature during transport toward the cell soma in primary neurons. J Cell Biol 196, 407–417.
Man HY, Lin JW, Ju WH, Ahmadian G, Liu L, Becker LE, Sheng M, Wang YT (2000). Regulation of AMPA receptor-mediated synaptic transmission by clathrin-dependent receptor internalization. Neuron 25, 649–662.
Margeta MA, Wang GJ, Shen K (2009). Clathrin adaptor AP-1 complex excludes multiple postsynaptic receptors from axons in *C. elegans*. Proc Natl Acad Sci USA 106, 1632–1637.
Maricq AV, Peckol E, Driscoll M, Bargmann CI (1995). Mechanosensory signalling in *C. elegans* mediated by the GLR-1 glutamate receptor. Nature 378, 78–81.
Martina JA, Bonangelino CJ, Aguilar RC, Bonifacino JS (2001). Stonin 2: an adaptor-like protein that interacts with components of the endocytic machinery. J Cell Biol 153, 1111–1120.
Matsuda S, Kakegawa W, Budisantoso T, Nomura T, Kohda K, Yuzaki M (2013). Stargazin regulates AMPA receptor trafficking through adaptor protein complexes during long-term depression. Nat Commun 4, 2759.
Matsuda S, Miura E, Matsuda K, Kakegawa W, Kohda K, Watanabe M, Yuzaki M (2008). Accumulation of AMPA receptors in autophagosomes in neuronal axons lacking adaptor protein AP-4. Neuron 57, 730–745.
McCormick PJ, Martina JA, Bonifacino JS (2005). Involvement of clathrin and AP-2 in the trafficking of MHC class II molecules to antigen-processing compartments. Proc Natl Acad Sci USA 102, 7910–7915.
McMahon HT, Boucrot E (2011). Molecular mechanism and physiological functions of clathrin-mediated endocytosis. Nat Rev Mol Cell Biol 12, 517–533.
Mellem JE, Brockie PJ, Zheng Y, Madsen DM, Maricq AV (2002). Decoding of polymodal sensory stimuli by postsynaptic glutamate receptors in *C. elegans*. Neuron 36, 933–944.
Mitsunari T, Nakatsu F, Shioda N, Love PE, Grinberg A, Bonifacino JS, Ohno H (2005). Clathrin adaptor AP-2 is essential for early embryonal development. Mol Cell Biol 25, 9318–9323.
Monteiro MI, Ahlawat S, Kowalski JR, Malkin E, Koushika SP, Juo P (2012). The kinesin-3 family motor KLP-4 regulates anterograde trafficking of GLR-1 glutamate receptors in the ventral nerve cord of *Caenorhabditis elegans*. Mol Biol Cell 23, 3647–3662.
Mullen GP, Grundahl KM, Gu M, Watanabe S, Hobson RJ, Crowell JA, McManus JR, Mathews EA, Jorgensen EM, Rand JB (2012). UNC-41/Stonin functions with AP2 to recycle synaptic vesicles in *Caenorhabditis elegans*. PLoS One 7, e40095.
Nonet ML, Holgado AM, Brewer F, Serpe CJ, Norbeck BA, Holleran J, Wei L, Hartwieg E, Jorgensen EM, Alfonso A (1999). UNC-11, a *Caenorhabditis elegans* AP180 homologue, regulates the size and protein composition of synaptic vesicles. Mol Biol Cell 10, 2343–2360.
Owen DJ, Collins BM, Evans PR (2004). Adaptors for clathrin coats: structure and function. Annu Rev Cell Dev Biol 20, 153–191.
Palmer CL, Lim W, Hastie PGR, Toward M, Korolchuk VI, Burbidge SA, Banting G, Collingridge GL, Isaac JTR, Henley JM (2005). Hippocalcin functions as a calcium sensor in hippocampal LTD. Neuron 47, 487–494.
Pan C-L, Baum PD, Gu M, Jorgensen EM, Clark SG, Garriga G (2008). *C. elegans* AP-2 and retromer control Wnt signaling by regulating mig-14/Wntless. Dev Cell 14, 132–139.
Pfaffl MW (2001). A new mathematical model for relative quantification in real-time RT-PCR. Nucleic Acids Res 29, e45.
Prekeris R, Klumperman J, Chen YA, Scheller RH (1998). Syntaxin 13 mediates cycling of plasma membrane proteins via tubulovesicular recycling endosomes. J Cell Biol 143, 957–971.
Ravikumar B, Sarkar S, Davies JE, Futter M, Garcia-Arencibia M, Green-Thompson ZW, Jimenez-Sanchez M, Korolchuk VI, Lichtenberg M, Luo S, *et al*. (2010). Regulation of mammalian autophagy in physiology and pathophysiology. Physiol Rev 90, 1383–1435.
Robinson MS (2004). Adaptable adaptors for coated vesicles. Trends Cell Biol 14, 167–174.
Rong Y, Liu M, Ma L, Du W, Zhang H, Tian Y, Cao Z, Li Y, Ren H, Zhang C, *et al*. (2012). Clathrin and phosphatidylinositol-4,5-bisphosphate regulate autophagic lysosome reformation. Nat Cell Biol 14, 924–934.
Rongo C, Whitfield CW, Rodal A, Kim SK, Kaplan JM (1998). LIN-10 is a shared component of the polarized protein localization pathways in neurons and epithelia. Cell 94, 751–759.
Shafaq-Zadah M, Brocard L, Solari F, Michaux G (2012). AP-1 is required for the maintenance of apico-basal polarity in the *C. elegans* intestine. Development 139, 2061–2070.
Shepherd JD, Huganir RL (2007). The cell biology of synaptic plasticity: AMPA receptor trafficking. Annu Rev Cell Dev Biol 23, 613–643.
Shim J, Lee J (2000). Molecular genetic analysis of *apm-2* and *aps-2*, genes encoding the medium and small chains of the AP-2 clathrin-associated protein complex in the nematode *Caenorhabditis elegans*. Mol Cells 10, 309–316.
Shim J, Lee J (2005). The AP-3 clathrin-associated complex is essential for embryonic and larval development in *Caenorhabditis elegans*. Mol Cells 19, 452–457.
Shim J, Sternberg PW, Lee J (2000). Distinct and redundant functions of mu1 medium chains of the AP-1 clathrin-associated protein complex in the nematode *Caenorhabditis elegans*. Mol Biol Cell 11, 2743–2756.
Simpson F, Peden AA, Christopoulou L, Robinson MS (1997). Characterization of the adaptor-related protein complex, AP-3. J Cell Biol 137, 835–845.
Strange K, Christensen M, Morrison R (2007). Primary culture of *Caenorhabditis elegans* developing embryo cells for electrophysiological, cell biological and molecular studies. Nat Protoc 2, 1003–1012.
Traub LM, Bannykh SI, Rodel JE, Aridor M, Balch WE, Kornfeld S (1996). AP-2-containing clathrin coats assemble on mature lysosomes. J Cell Biol 135, 1801–1814.
Unoki T, Matsuda S, Kakegawa W, Van NTB, Kohda K, Suzuki A, Funakoshi Y, Hasegawa H, Yuzaki M, Kanaho Y (2012). NMDA receptor-mediated PIP5K activation to produce PI(4,5)P2 is essential for AMPA receptor endocytosis during LTD. Neuron 73, 135–148.
Walther K, Diril MK, Jung N, Haucke V (2004). Functional dissection of the interactions of stonin 2 with the adaptor complex AP-2 and synaptotagmin. Proc Natl Acad Sci USA 101, 964–969.
Wang YT, Linden DJ (2000). Expression of cerebellar long-term depression requires postsynaptic clathrin-mediated endocytosis. Neuron 25, 635–647.
Watt SA, Kular G, Fleming IN, Downes CP, Lucocq JM (2002). Subcellular localization of phosphatidylinositol 4,5-bisphosphate using the pleckstrin homology domain of phospholipase C δ1. Biochem J 363, 657–666.
Yoon B-J, Smith GB, Heynen AJ, Neve RL, Bear MF (2009). Essential role for a long-term depression mechanism in ocular dominance plasticity. Proc Natl Acad Sci USA 106, 9860–9865.
Zhang B, Koh YH, Beckstead RB, Budnik V, Ganetzky B, Bellen HJ (1998). Synaptic vesicle size and number are regulated by a clathrin adaptor protein required for endocytosis. Neuron 21, 1465–1475.
Zhang D, Isack NR, Glodowski DR, Liu J, Chen CCH, Xu XZS, Grant BD, Rongo C (2012). RAB6.2 and the retromer regulate glutamate receptor recycling through a retrograde pathway. J Cell Biol 196, 85–101.
Zheng Y, Brockie PJ, Mellem JE, Madsen DM, Maricq AV (1999). Neuronal control of locomotion in *C. elegans* is modified by a dominant mutation in the GLR-1 ionotropic glutamate receptor. Neuron 24, 347–361.
Zheng Y, Mellem JE, Brockie PJ, Madsen DM, Maricq AV (2004). SOL-1 is a CUB-domain protein required for GLR-1 glutamate receptor function in *C. elegans*. Nature 427, 451–457.